Bachelor Thesis

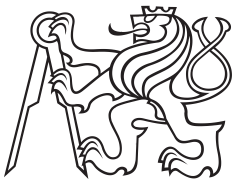

Czech Technical University in Prague

F3

Faculty of Electrical Engineering
Department of Control Engineering

Vehicle brake system development

Vojtěch Ullmann

Supervisor: doc. Ing. Tomáš Haniš, Ph.D.
Field of study: Cybernetics and Robotics
May 2023

BACHELOR‘S THESIS ASSIGNMENT

I. Personal and study details

Student's name: **Ullmann Vojtěch** Personal ID number: **499179**

Faculty / Institute: **Faculty of Electrical Engineering**

Department / Institute: **Department of Control Engineering**

Study program: **Cybernetics and Robotics**

II. Bachelor’s thesis details

Bachelor’s thesis title in English:

Vehicle brake system development

Bachelor’s thesis title in Czech:

Vývoj brzdného systému vozu

Guidelines:

The primary goal of the thesis is to develop and implement modular vehicle brake system allowing for independent wheel actuation. The braking system will build on previously developed brake by wire concept.
1. Get familiar with vehicle dynamics and brake systems models and implement suitable model.
2. Get familiar with automotive electric brake boosters.
3. Develop and implement brake by wire system.
4. Evaluate developed brake system.

Bibliography / sources:

[1] Dieter Schramm, Manfred Hiller, Roberto Bardini – Vehicle Dynamics – Duisburg 2014
[2] Hans B. Pacejka - Tire and Vehicle Dynamics – The Netherlands 2012
[3] Robert Bosch GmbH - Bosch automotive handbook - Plochingen, Germany : Robet Bosch GmbH ; Cambridge, Mass. : Bentley Publishers
[4] Rajamani R. (2012) Mean Value Modeling of SI and Diesel Engines. In: Vehicle Dynamics and Control. Mechanical Engineering Series. Springer, Boston, MA. https://doi.org/10.1007/978-1-4614-1433-9_9

Name and workplace of bachelor’s thesis supervisor:

doc. Ing. Tomáš Haniš, Ph.D. Department of Control Engineering FEE

Name and workplace of second bachelor’s thesis supervisor or consultant:

Date of bachelor’s thesis assignment: **31.01.2023** Deadline for bachelor thesis submission: **26.05.2023**

Assignment valid until:
by the end of summer semester 2023/2024

doc. Ing. Tomáš Haniš, Ph.D.	prof. Ing. Michael Šebek, DrSc.	prof. Mgr. Petr Páta, Ph.D.
Supervisor’s signature	Head of department’s signature	Dean’s signature

III. Assignment receipt

The student acknowledges that the bachelor’s thesis is an individual work. The student must produce his thesis without the assistance of others, with the exception of provided consultations. Within the bachelor’s thesis, the author must state the names of consultants and include a list of references.

. | _____
Date of assignment receipt | Student’s signature

Acknowledgements

Above everyone, I am very thankful to my supervisor, doc. Ing. Tomáš Haniš, Ph.D., for his time, friendly attitude, and immediate answers.

My immense gratitude belongs to my parents for their support and for making my studies possible.

Also, I want to thank all my colleagues in the Smart Driving Solutions research group for their friendly and helpful attitude. Last but not least, I would like to thank Zdeněk Eisner for providing me toolbox and quick tips.

Declaration

I declare that the presented work was developed independently and that I have listed all sources of information used within it in accordance with the methodical instructions for observing the ethical principles in the preparation of university theses.

In Prague, May 26th 2023 .....

Abstract

This bachelor's thesis offers an overview of brake systems in the automotive industry. A particular focus is given to electric brake boosters, which are nowadays among the closest fail-safe solutions for the brake-by-wire concept. Then one of these devices – the second generation of Bosch's iBooster is analyzed for possible modification as an independent wheel brake actuator for still the essential frictional braking with a hydraulic system. Various strategies for commanding the iBooster are presented. However, direct control with a motor controller proves to be the most suitable and is further developed for the final solution of this thesis. Finally, the control law is established and evaluated on the adopted twin-track model in a common traffic scenario. The results are further discussed even for a complication caused by the hydraulics system.

Keywords: Automotive brake systems, Brake-by-Wire, electric brake boosters, electrohydraulic brakes

Supervisor: doc. Ing. Tomáš Haniš, Ph.D.
Czech Technical University in Prague,
Faculty of Electrical Engineering,
Department of Control Engineering,
Karlovo náměstí 13,
121 35 Praha 2 - Nové Město

Abstrakt

Tato bakalářská práce poskytuje přehled brzdových systémů v automobilovém průmyslu. Zvláštní pozornost je věnována elektrickým posilovačům brzd, které jsou dnes nejbliže implementaci brake-by-wire systému i po bezpečnostní stránce. Poté je analyzováno jedno z těchto zařízení – druhá generace iBooster od společnosti Bosch – z hlediska možnosti modifikace na nezávislý brzdový aktuátor pro stále nezbytné třecí brzdy s hydraulickým systémem. Za tim účelem jsou představeny různé strategie pro řízení iBoosteru. Ukazuje se, že přímé řízení pomocí budiče elektromotoru se ukazuje jako nejvhodnější a je tedy zvoleno pro vývoj konečného řešení této práce. Nakonec je navržen a vyhodnocen řídící algoritmus na přejatém dvoustopém modelu vozidla simulující běžnou situaci v dopravě. Výsledky jsou dále diskutovány i kvůli komplikaci způsobené hydraulikým systémem.

Klíčová slova: Brzdný systém automobilu, Brake-by-Wire, elektrické posilovače brzd, elektrohydraulické brzdy

Překlad názvu: Vývoj brzdného systému vozu

Contents

Figures

Tables

Abbreviations

ABS Antilock Braking System

BbW Brake-by-Wire

CAN Controller Area Network

CoG Centre of Gravity

DbW Drive-by-Wire

ESP Eletronic Stability Program

PMSM Permanent Magnet Synchronous Motor

PWM Pulse Width Modulation

SbW Steer-by-Wire

SDS Smart Driving Solutions

SENT Single Edge Nibble Transmission

SISO Single Input and Single Output

TbW Throttle-by-Wire

TMC Tandem Master Cylinder

WSS Wheel Speed Sensor

Chapter 1

Introduction

1.1 Motivation

The automotive industry has been facing many challenges in recent years. The first is the situation of supply chain shortage due to covid-19 pandemic. Furthermore, the industry can not know how long the excess demand will withstand inflation and recession on potential customers [1, 2]. Last but not least, large economies require to follow specific regulations on their territory by 2025, e.g., proposed Euro 7 (the EU), LEV III (California) + Federal 'Tier 3' Standards (the USA) [3], China 6 (China) [4], Proconve L8 (Brazil) [5]. All struggles listed above stress the necessity of constant research and development at all levels in the industry.

At the Czech Technical University in Prague, we have a special SDS research team aiming to enhance the driving experience through the concept of an over-actuated vehicle with independent wheel units, as illustrated in the picture 1.1. The vision of improving the drivability of modern vehicles is inspired by the well-known Fly-by-Wire solution in the aerospace industry, in which this approach has outperformed direct control of mechanical and hydraulic systems. These control systems, generally called Drive-by-Wire (DbW), consist of the following subsystems:

- Brake-by-Wire (BbW)
- Steer-by-Wire (SbW)
- Throttle-by-Wire (TbW)
- Shift-by-Wire

Establishing advanced relationships between these systems will allow the merge of data from sensors and opt for the most efficient command of a higher system (driver or autonomous driving system in the future).

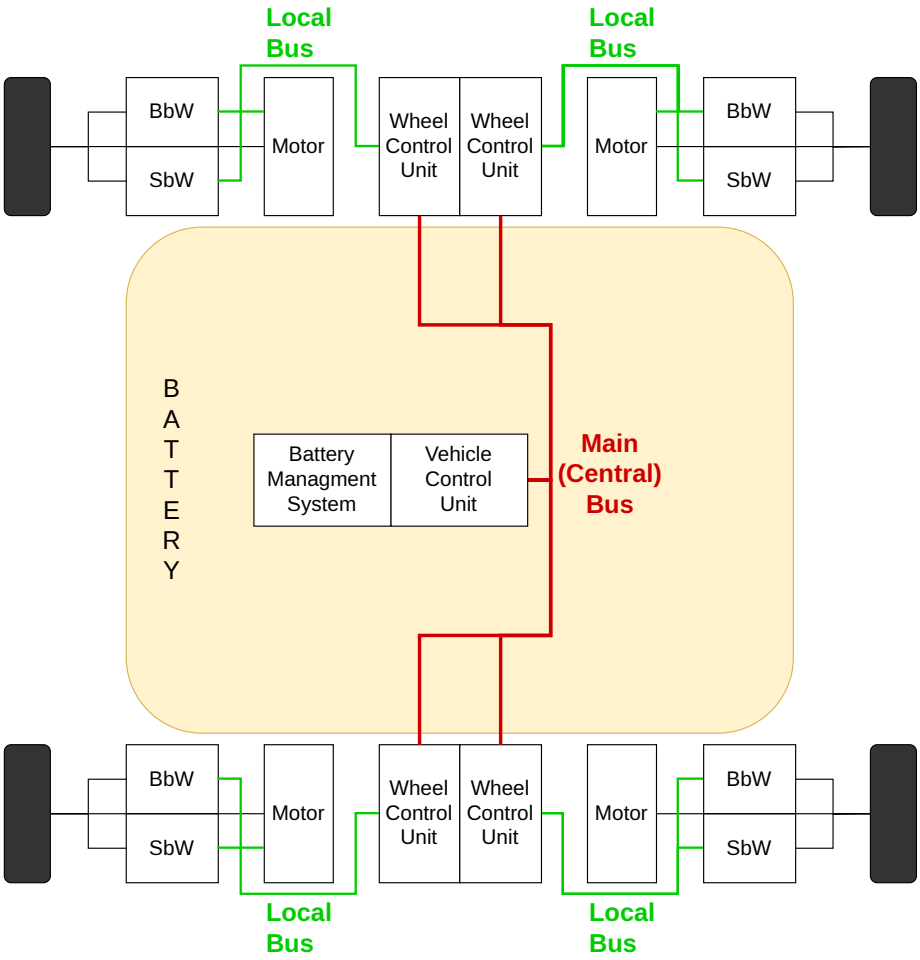

Figure 1.1: Diagram of Smart Driving Solutions (SDS)'s concept vehicle

Our primary regulation of interest is the proposed Euro 7 regulation. It is necessary to note that the Euro 7 regulation's details are still in negotiation and thus can differ in the final form. Nonetheless, the broader area of interest in this proposal can be considered inevitable, from only setting the upper bounds of emissions, like in previous standards, to complex limitations of pollution caused by a vehicle. The proposal includes, most importantly, evaporative emissions from brakes and tires and defines battery durability [6].

1.2 Outline

This thesis aims to present brake systems used in the automotive industry and create a hydraulic actuator for BbW systems based on the automotive-grade electric brake booster.

Chapter 2

Vehicle Brake Systems

2.1 Hydraulic Brake Systems

Throughout the years, the aerospace and automotive industries converged to hydraulic brakes as their standard method of stopping wheels. This preference is driven by the advantages of hydraulics, such as

- Ability to transfer large forces
- Relatively immediate response
- Reliability
- Simplicity
- Durability (minor damage to a hydraulic line should not result in immediate failure)

Disadvantages appear in more complex hydraulic systems where lines can be too long and introduce a transport delay, and also, the mass of the whole system becomes a concern. It is also necessary to mention that most fluids used in hydraulic systems are toxic to the environment and living beings. Although these negative aspects of hydraulic systems can seem severe, overcoming them and integrating hydraulic-based solutions is not complicated for today's state of engineering.

Figure 2.1 depicts the physical principle behind hydraulic brakes. It shows the assumption of constant hydraulic pressure in enclosed hydraulic fluid. This phenomenon is known as Pascal's principle, whose application implies the following equation

$$\frac{F_1}{A_1} = \frac{F_2}{A_2}. \tag{2.1}$$

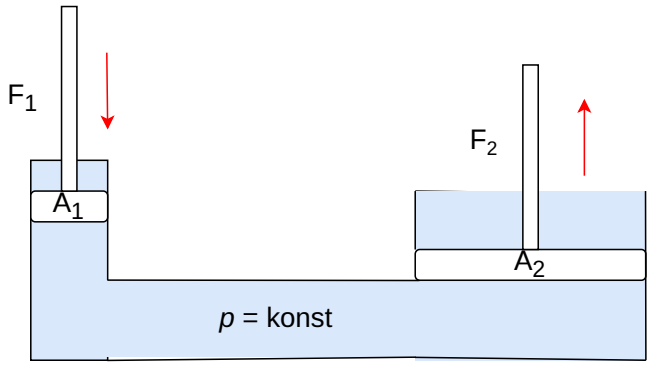

Figure 2.1: Pascal's Principle

2.1.1 Mechanical Hydraulic Brake Systems

Mechanical hydraulic brakes are today's vehicles' most commonly used brake system. There is tremendous experience with their application, and as shown in figure 2.2, the mechanical brake system is simple and thus cost-effective [7]. It contains only a comfortable brake booster, Tandem Master Cylinder (TMC), brake lines, and the wheels' brakes. Nowadays, the system is extended with a mandatory Antilock Braking System (ABS) unit for safety reasons.

Another safety concern instructs us which wheels should be connected in the split braked system. The diagonally split option in passenger vehicles is used because it secures the smallest stability drop when one line fails [8]. On the other hand, front-and-rear split gained popularity in motorsport for uncomplicated application, modifications and lower mass.

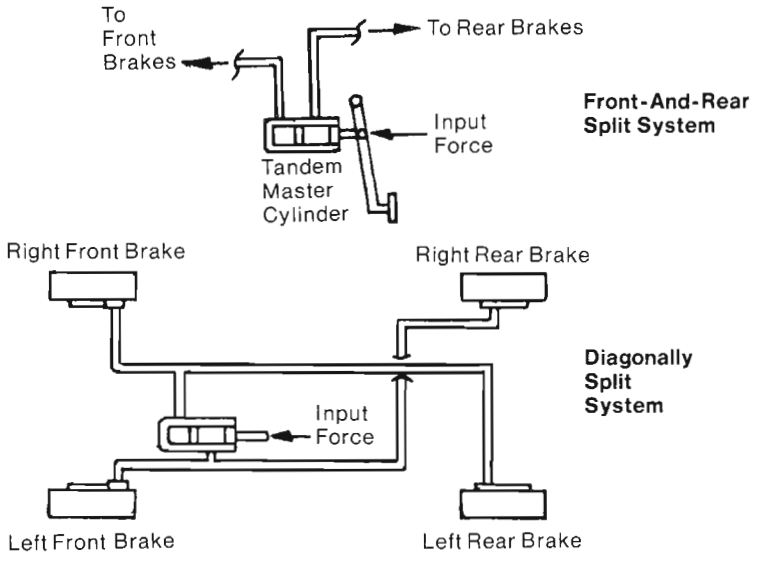

Figure 2.2: Basic hydraulic brake system diagram. Adopoted from [9]

2.1.2 Electrohydraulic Brake Systems

This system builds on the reliable system introduced in the previous section. The key difference is that an electronic control unit and a hydraulic modulator are added. TMC is disconnected from the hydraulic circuit by isolating valves. The control unit reads the demanded pressure from the particular sensor or position sensor.

The pedal feels imitation is often implemented. The benefit of this approach is that the reference value is processed by a complex control algorithm, which can consider data from the accelerometer or Wheel Speed Sensor (WSS) and hence compute the optimal amount of hydraulic pressure to guarantee the vehicle's overall stability, like Eletronic Stability Program (ESP) [8].

Besides, the control unit allows us to use, for example, Controller Area Network (CAN) bus and report the status to the rest of the car. In case of a malfunction or error, the system connects the isolating valves to the hydraulic system and thus providing an alternative setup for safety. Electric brake boosters and integrated power brakes (introduced below) are classic representatives of electrohydraulic solutions.

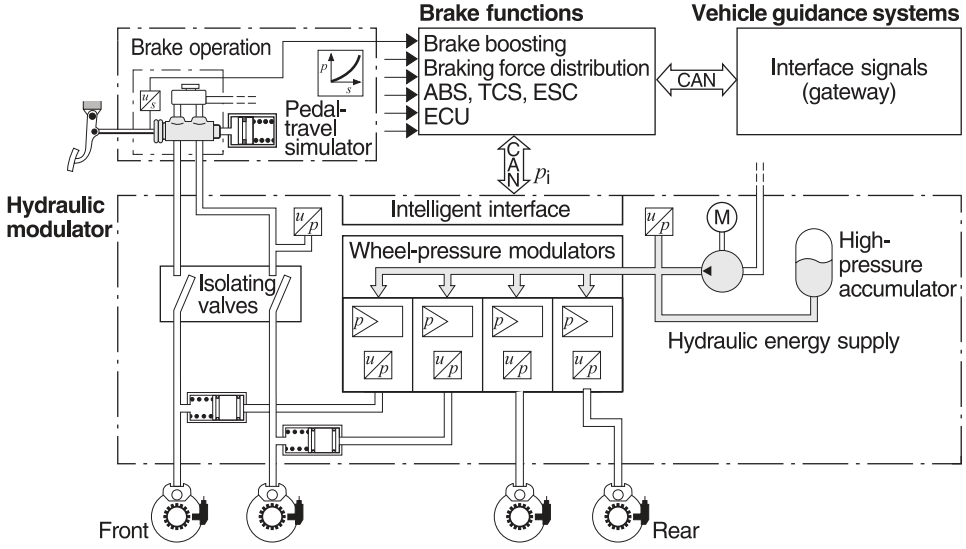

Figure 2.3: Electrohydraulic brake system. Adopted from [8]

2.2 Electromechanical Brake Systems

The electromechanical principle would be the closest to the BbW idea. However, the current state of the art does not offer a brake system like this in accordance with functional safety legislation. Although they cannot be used as the primary braking actuator, it is legal to equip a handbrake like in figure 2.4. These actuators can potentially help to hill climb assist or stop the vehicle in case of emergency braking.

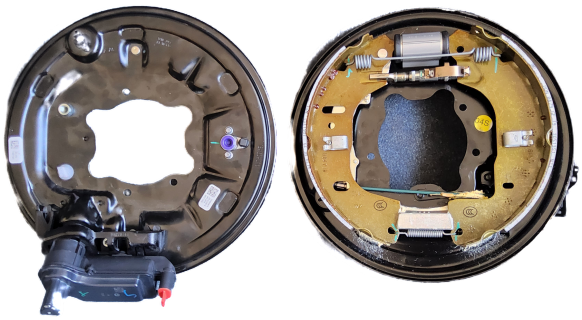

Figure 2.4: Electromechanical brake example

2.3 Brake Boosters

2.3.1 Vacuum Brake Booster

If we tried just to press the TMC, it would be difficult to reach and hold the brake pedal in a single position all the time. The vacuum booster amplifies the user's demanded deceleration. This amplification has become so popular that nowadays, this kind of booster is spread in every vehicle with internal combustion. For a detailed description, see [9].

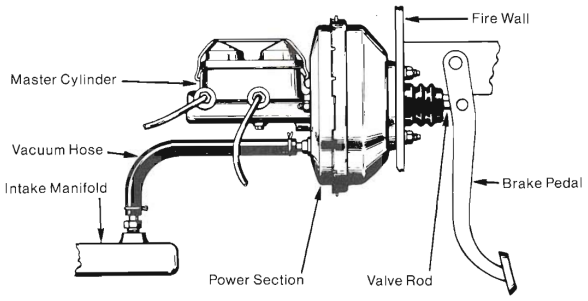

Figure 2.5: Standard Vacuum brake booster. Adopted from [9]

Brake boosters based onthe vacuum are in every gasoline vehicle because gasoline engines create a vacuum. However, diesel, hybrid, and electric cars cannot create a vacuum. The solution is as simple as adding a hydraulic pump or using a hydraulic booster (which I do not discuss further because of their lesser relevance, if interested, see [9]).

2.3.2 Electric Brake Booster

Like the previously mentioned vacuum brake booster, the primary task of this equipment is to make pressing the brake pedal more comfortable for drivers. Ordinarily, the device can be divided into two essential parts – the pedal sensor and TMC. The pedal sensor is present to give an authentic feeling and determine how much a Permanent Magnet Synchronous Motor (PMSM) (typically) should support the press [8].

The difference is electric brake boosters are more customizable. For example, the pedal feels according to the driving mode. Also, they support the system with an ESP unit. In this setup, the electric brake booster offers an additional level of redundancy because it can process data from WSS. Also, electric brake boosters can brake without input from the driver in case of an emergency.

Another benefit is its compact size and low mass. It is also common practice that electric brake boosters are connected to their own ESP unit. Figure 2.6 shows the solution of integrated power brake by Continental. The more detailed description of the operation is in 4. The rest is well described in [8].

Figure 2.6: Electric Brake Booster. Adopoted form [10]

2.4 Other Means of Deceleration

- **Regenerative Braking** – The electric motor is used as a generator. This process is effective at medium and higher speeds [8].
- **Aerodynamic Braking** – Active wing changes the drag coefficient and slows the car at higher speeds [9, 11].
- **Brake-by-Steer** – Instead of frictional brakes, the friction of tires is used to completely stop the car from lower speeds [12].

Chapter 3

Vehicle Dynamics Modeling

3.1 Overview

Nowadays, it is not necessary and, from an economic perspective, even acceptable to start the development of new systems in the real world as computational power has become very powerful. Everything began in 1940 with the first single-track model [11].

The model stated several simplifications, to name a few: constant longitudinal velocity of the vehicle's Centre of Gravity (CoG), neglected rotational motions around the CoG except for yaw, all mass is situated in the CoG, the front and rear tires are merged into one wheel for each axle, and limitations implicated by these assertions [11]. All restrictions leave the single-track model with only two degrees of freedom. Although this model suits well for simulating longitudinal dynamics, the results will be outperformed with a well-identified twin-track model.

The twin-track model offers at least twice (14 DoF) as many degrees of freedom compared to the advanced version of the single-track (7 DoF). These parameters cover most of the needs for control system designs while keeping the computational time requirements low [11]. For a detailed examination of forces and torques, there are advanced techniques for dealing with multibody systems models, which consist of hundreds of parameters [11].

This thesis adopts a twin-track model based on [13] that was extended with a high-level braking system control in [12], see figure 3.1. In contrast with the single-track model, this option offers a broad spectrum of parameters and an accurate description of forces and torques on individual tires. The rest of this chapter briefly describes the adopted twin-track model and focuses on several quantities which play a particular role in brake systems. Parts like suspension will not be discussed, and in case of interest, see [13].

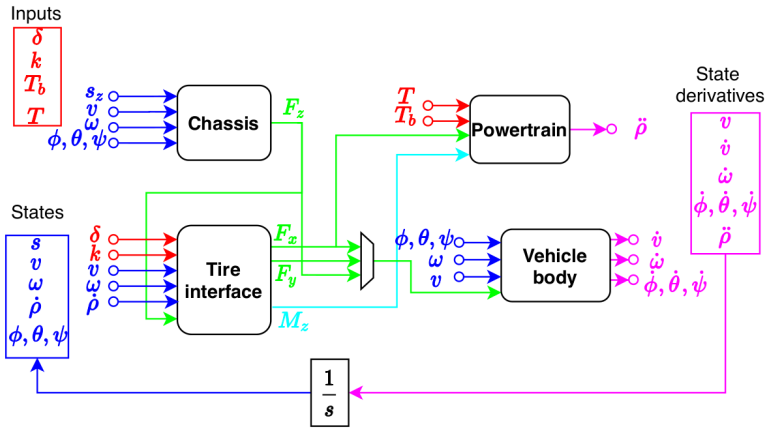

Figure 3.1: Illustrative scheme of the twin-track model. Adopted from [12]

3.2 Motion

The vehicle's motion can be described with the following Newtonian equations in vector form

$$m_{\mathrm{V}}\ddot{\boldsymbol{r}}_{\mathrm{V}} = \sum_{i=1}^{4} \boldsymbol{F}_i - m_{\mathrm{V}} g \boldsymbol{e}_z + \boldsymbol{F}_{\mathrm{W}}, \tag{3.1}$$

where m_{V} is the vehicle's total mass, $\boldsymbol{r}_{\mathrm{V}}$ stands for position vector, g is the gravitational constant with the z-axis's unity vector $\boldsymbol{e}_z$, $\boldsymbol{F}_{\mathrm{W}}$ represents air resistance and aerodynamic forces and $\boldsymbol{F}_i$ are forces transmitted between wheel suspension and the chassis [11].

The equation (3.1) is further expanded into the following form with unrolled vectors for better insight

$$m_{\mathrm{V}} \left(\begin{bmatrix} \dot{v}_x \\ \dot{v}_y \\ \dot{v}_z \end{bmatrix} + \boldsymbol{\omega}_{\mathrm{V}} \times \begin{bmatrix} v_x \\ v_y \\ v_z \end{bmatrix} \right) = \sum_{i=1}^{4} \begin{bmatrix} F_{\mathrm{R}_i,x} \\ F_{\mathrm{R}_i,y} \\ F_{\mathrm{R}_i,z} \end{bmatrix} - \begin{bmatrix} 0 \\ 0 \\ m_{\mathrm{V}} g \end{bmatrix} - \frac{1}{2} c_{\mathrm{W}} \rho A \left\| \boldsymbol{v} \right\|_2 \begin{bmatrix} v_x \\ v_y \\ 0 \end{bmatrix}, \tag{3.2}$$

where $\boldsymbol{\omega}_{\mathrm{V}}$ is the absolute angular velocity of the chassis, $v_{x/y/z}$ are vehicle body speed in the given axis, c_{W} is a drag coefficient, ρ symbolizes air density and A is surface area exposed to air flow. The figure 3.2 describes forces and coordinate systems from the previous equations.

In the next step, the model requires the description of rotational motion. These equations are called Euler's equations (3.3), whose purpose is to sum all torques affecting the vehicle.

$$\boldsymbol{J}_{\mathrm{V}} \dot{\boldsymbol{\omega}}_{\mathrm{V}} + \boldsymbol{\omega}_{\mathrm{V}} \times (\boldsymbol{J}_{\mathrm{V}} \boldsymbol{\omega}_{\mathrm{V}}) = \sum_{i=1}^{4} (\boldsymbol{r}_i \times \boldsymbol{F}_i) + \boldsymbol{r}_{\mathrm{W}} \times \boldsymbol{F}_{\mathrm{W}}, \tag{3.3}$$

where $\boldsymbol{J}_{\mathrm{V}}$ is the inertia matrix of the chassis, $\boldsymbol{r}_i$ represents the points where the $\boldsymbol{F}_i$ act and $\boldsymbol{r}_{\mathrm{W}}$ is the centre of aerodynamic pressure [11].

The last presented equation (3.4) explains the acceleration of the i-th wheel.

$$J_{\mathrm{R}_i} \ddot{\rho}_{\mathrm{R}_i} = T_{\mathrm{d}_{\mathrm{R}i}} - T_{\mathrm{b}_{\mathrm{R}_i}} \operatorname{sign}(\dot{\rho}_{\mathrm{R}_i}) - r_{\mathrm{R}_i} F_{\mathrm{R}_i,x}, \tag{3.4}$$

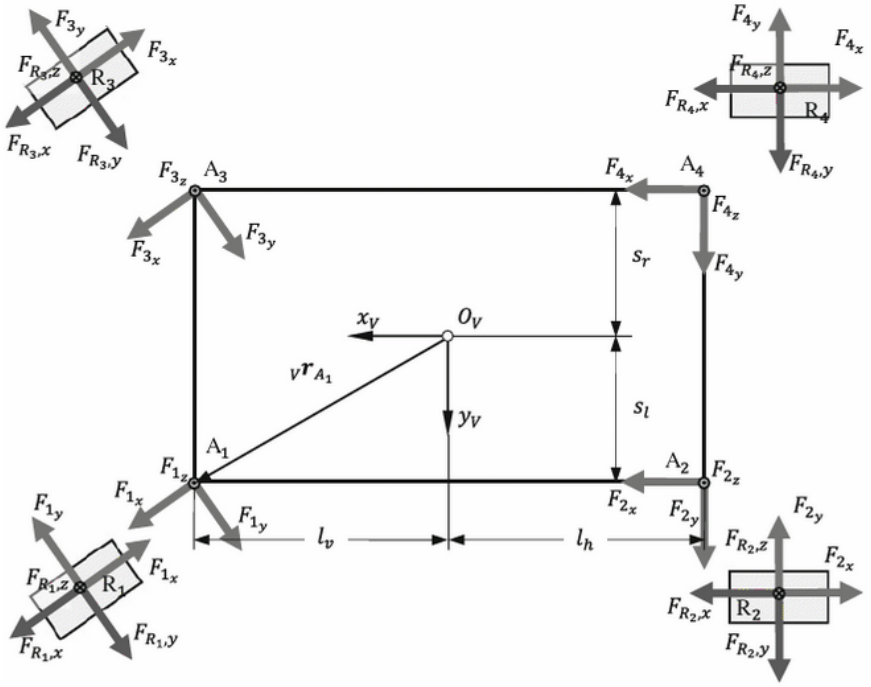

Figure 3.2: Free body diagram of a twin-track model. Adopted from [11]

where J_{R_i} is wheel's moment of inertia, ρ_{R_i} is wheel's angular velocity, $T_{\mathrm{dR}i}$ represents driving torque on the wheel, $T_{\mathrm{b}_{\mathrm{R}_i}}$ is braking torque on the wheel, r_{R_i} is wheel's radius and $F_{\mathrm{R}_i,x}$ symbolizes longitudinal force on the wheel [11].

3.3 Tire Model

The longitudinal slip is defined as

$$\lambda_i = \frac{v_{\mathrm{R}_i,x} - r_{\mathrm{R}_i}\dot{\rho}_{\mathrm{R}_i}}{\max\left(\left|v_{\mathrm{R}_i,x}\right|, \left|r_{\mathrm{R}_i}\dot{\rho}_{\mathrm{R}_i}\right|\right)}, \tag{3.5}$$

where $v_{\mathrm{R}_i,x}$ is measured in the center of the wheel. And finally, the slip angle equals to

$$\alpha_i = -\arctan\left(\frac{v_{\mathrm{R}_i,y}}{\max\left(\left|v_{\mathrm{R}_i,x}\right|, \left|r_{\mathrm{R}_i}\dot{\rho}_{\mathrm{R}_i}\right|\right)}\right). \tag{3.6}$$

Among the most recognized tire models is the *Magic Formula Model*. Hans Pacejka invented the formula and improved it over time. Hence, there are countless considerations described in [14] for the final model to adjust it perfectly to our needs and testing scenario. However, the adopted twin-track model uses a simplified version of the magic formula.

$$F_x(\lambda) = D\sin\left(C\arctan\left(B\lambda - E\left(B\lambda - \arctan B\lambda\right)\right)\right), \tag{3.7}$$

with constant parameters D, C, B, and E. The argument of the function λ is longitudinal slip. If we had wanted to model slip angle α for lateral force F_y, all we would have had to do is to swap λ with α in the equation (3.7) [14].

The so-called friction ellipse in figure 3.3 visualizes the relationship between longitudinal and lateral forces based on the abovementioned parameters. Otherwise, the magic formula would keep the forces independent of each other, and that does not correspond with observations in reality. The more profound analysis of how to calculate these forces and their maximums is shown in [11]. In real-world systems, the application of these indicators lies in stability assistants like ESP.

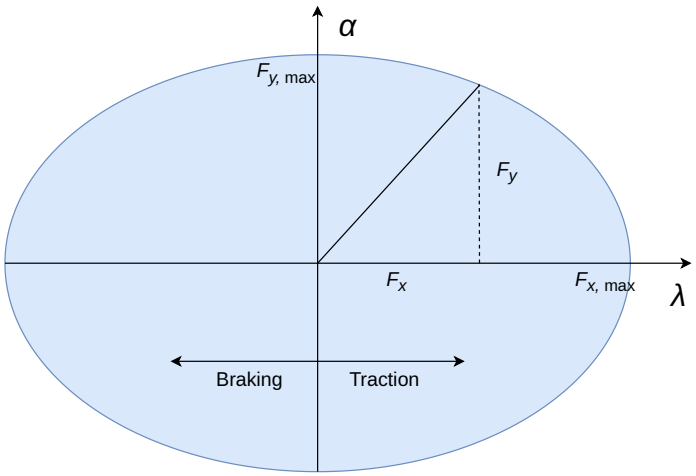

Figure 3.3: Friction ellipse

3.4 Brakes

The last step of this chapter is an example of how is vehicle dynamics connected with the low-level brake system. The longitudinal force in the case of the straight motion on an ideal surface, accordingly to Newton's second law, equals

$$F_x = ma_x. \tag{3.8}$$

Now we want to know the force on a single wheel. To calculate this, we need to divide the longitudinal force by the brake force distribution *dist* between axles and also by the number of wheels on the axle, as shown here

$$F_{\mathrm{R_i,x}} = \frac{F_x dist}{2}. \tag{3.9}$$

Then the torque on a wheel can be calculated simply as

$$T_{\mathrm{R}_i} = F_{\mathrm{R_i,x}} r_{\mathrm{R}_i}. \tag{3.10}$$

To know the required hydraulic pressure, we need to state the type of brake. For simplicity, the final equation will be demonstrated on the most common disc brakes. The upcoming formula represents the force on the disc.

$$F_{\mathrm{disc}} = \frac{T_{\mathrm{R}_i}}{r_{\mathrm{disc_{eff}}}}. \tag{3.11}$$

Last but not least, it is necessary to write the equation of the force on the pad

$$F_{\text{pad}} = \frac{F_{\text{disc}}}{2\mu_{\text{pad}}}, \tag{3.12}$$

and thus we are able to compute the hydraulic pressure through following equation

$$p = \frac{F_{\text{pad}}}{A_{\text{cp}}} = \frac{4F_{\text{pad}}}{\pi d_{\text{cp}}^2}. \tag{3.13}$$

Now it is possible to merge all equations and get the final definition of the brake torque below

$$T_{\text{R}_i} = 2pA_{\text{cp}}r_{\text{disc}_{\text{eff}}}\mu_{\text{pad}}\left(p, \vartheta\right), \tag{3.14}$$

where I consider the caliper to press both sides of the pad, p is the hydraulic pressure, A_{cp} is the area of the piston in caliper, $r_{\text{disc}_{\text{eff}}}$ is the effective radius, which equals to

$$r_{\text{disc}_{\text{eff}}} = r_{\text{disc}} - \frac{h_{\text{pad}}}{2}, \tag{3.15}$$

where r_{disc} represents the radius of the brake disc and h_{pad} is the height of the brake pad and finally the $\mu_{\text{pad}}\left(p, \vartheta\right)$ is the friction coefficient between the pads and disc, which depends on pressure p and temperature ϑ. This parameter is dynamic and it is possible to approximate it with these parabolas

$$\mu_{\text{pad}}\left(p, \vartheta\right) = \mu_{\text{pad},p=0}\left(1 - c_{\text{T}}\left(\frac{p}{p_{\text{max}}}\right)^2\right) \cdot \mu_{\text{pad,max}}\left(1 - c_{\text{P}}\left(\frac{\vartheta - \vartheta_{\text{opt}}}{\vartheta_{\text{opt}}}\right)^2\right), \tag{3.16}$$

where c_{T} and c_{P} are material constants and the ϑ_{opt} is the optimum temperature [11].

Chapter 4

Braking System Development

The main challenge of this project is to create a suitable low-level system for building pressure for braking and use in an actual vehicle. There has been a proof of concept prototype already with promising results (see [15]). However, there were concerns the lever mechanism could get loose or suffer from wear down over time. For this reason, we would like to use standard automotive components. Last but not least, it is essential to point out that this work is not an ambition to develop a production-ready solution; hence, not all redundancy elements are implemented, and the proposed solution is not fully compliant with legislation [16].

4.1 Actuator

There are several demands on a braking actuator from our side:

- Durability
- Compact size
- Controllability
- Space for redundancy
- Availability

Firstly, every possible automotive solution fulfills durability and redundancy. What had become a significant concern was availability. As mentioned in 1.1, the automotive industry is facing supply shortages, and thus not everyone can offer support for our needs. After months of research and negotiations with companies, we acquired actuators based on two operating principles.

The first is Bosch's iBooster (see figure 4.1a and mentioned in 2.3.2), which is widely spread among hybrid and electric vehicles in Europe, and the second is a standard ESP unit (see figure 4.1b). The iBooster allows broader possibilities for control but lacks behind the ESP unit in size comparison. As stated previously, the developed system will be used for experimental purposes, thence; it is beneficial to favor controllability as the most crucial demand.

The problem with the ESP unit is the complexity of pressure control. The pressure is increased or decreased by a set of solenoid valves. Moreover, regulated pressure depends on a hydraulic pump which builds the hydraulic pressure in the system. These system inputs would have to be considered during control law design. Control system design methods, which utilize multiple system inputs optimally, are advanced and beyond the scope of the bachelor program. On the other hand, iBooster can be controlled via classic methods for Single Input and Single Output (SISO) systems.

(a) : iBooster by Bosch

(b) : ESP unit

Figure 4.1: Available actuators

4.1.1 Bosch's iBooster (Gen. 2)

The second generation of Bosch's iBooster became more compact than the previous generation. The official information claims the overall to be between 4.4–4.8 kg. The device targets hybrid and electric vehicles, substituting conventional vacuum brake boosters. For this reason, the required space in the vehicle is almost identical. The power consumption of this device should be less than one ampere per ten bars. The supply voltage range (9.8–16 V) respects the traditional supply voltage of 12 V used in most cars. For more details, see [17, 18].

Controlling the iBooster via CAN bus

Controlling the device with CAN bus messages should be possible and function straightforwardly. Nevertheless, these messages are confidential, and they were received after the time when the decision for approach had to be taken for further work. Also, the iBooster accepts multiple CAN messages, and their correct order must be determined for proper operation. This process demands plenty of time that I could not afford to spend. In addition to complications with the communication, the software inside the control unit is unknown, making any chance of predicting the device's behavior impossible.

Using pedal sensor for controlling the iBooster

In real-world use cases, the input rod in 4.2 is connected to a brake pedal. When a driver pushes the pedal, the differential sensor measures the change in distance between the input rod and the boost body. The control unit, also shown in 4.2, processes data from the sensor and commands a PMSM to move with the boost body to follow the input rod's displacement and decrease it back to zero [19].

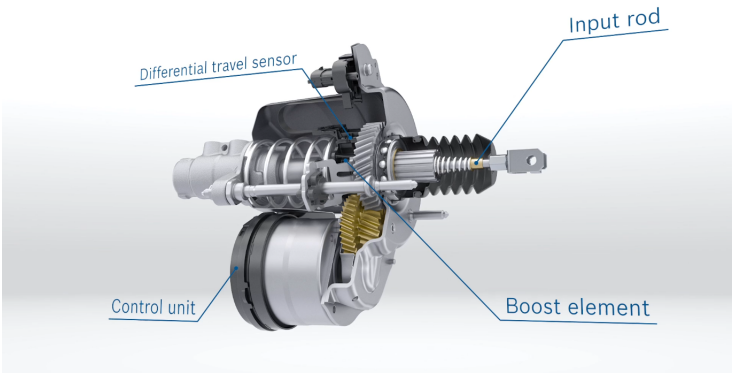

Figure 4.2: Cut through iBooster. Adopted from [18]

This mechanism had been the planned initial approach for control. However, I did not receive any further documentation; hence, I had to focus on the experiments of hobbyists and mechanics like [20]. Nonetheless, testing pinout with an oscilloscope and diode tester was still necessary. Figure 4.3 and table 4.1 show the discovered wiring, which allowed for providing the supporting force and pushing the input rod by hand.

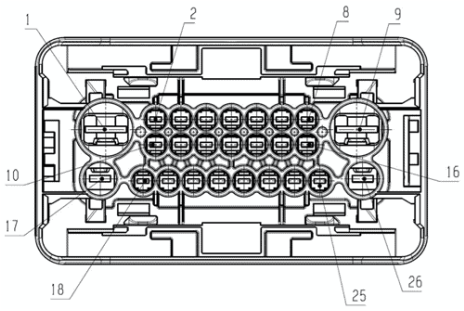

(a) : Connector of the Control Unit

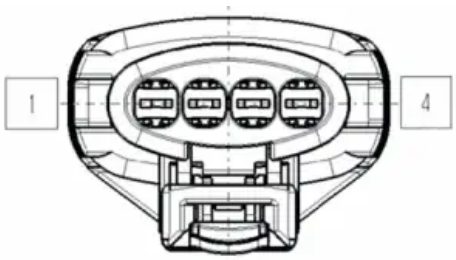

(b) : Connector of the Pedal Sensor

Figure 4.3: Wiring of the iBooster. Adopted from [20]

Another step was mimicking the output of the differential travel sensor. The data from the sensor is separated between two wires, as in figure 4.4–the first carried data as a 1 kHz Pulse Width Modulation (PWM) signal with a variable duty cycle. No movement corresponded to approximately a little less than 50 %. Pushing the input rod increased the duty, and releasing decreased it. The behavior of this signal seemed promising for the expected approach.

Signal's Name	Control Unit	Pedal Supply
+12 V	1	—
Pedal sensor supply	8	3
GND	9	—
CAN-L	16	—
Ignition (+12 V)	20	—
Pedal Sensor Signal 1	22	2
Pedal Sensor Signal 2	23	4
CAN-H	25	—
Pedal sensor GND	26	1

Table 4.1: Final Wiring of the iBooster [20]

However, the second signal stayed a mystery for a long time. Measurements showed it is a simplex communication from the sensor. As the first PWM signal did not reflect the level changes in transmission, I could exclude the theory that it can be a clock signal. At first, I unsuccessfully attempted to use all protocol decoders in *PulseView* (an open-source logic analyzer software) for one-wire buses, e.g., 1–Wire and Local Interconnect Network. Another point of view was checking whether the signal corresponds to some kind of code, e.g., (Differential) Manchester encoding, but undefined sequences were found during manual decoding.

Finally, after a long research on automotive buses, I encountered the Single Edge Nibble Transmission (SENT) protocol (SAE J2716). The protocol's main strengths are simplicity (it does not require special peripherals but an ordinary timer), multiple ways of detecting errors in some packet formats, and speed. SENT protocol is based on measuring the number of ticks between falling edges. Every transmission starts with a calibration pulse whose time length t_{calib} is divided by a magic constant of 56. The result gives us one tick of the message. Then every pulse represents a nibble–the equation (4.1) presents the nibble's calculation from a pulse of a time length t

$$nibble_{\text{val}} = \frac{t}{t_{\text{tick}}} - 12 = 56 \cdot \frac{t}{t_{\text{calib}}} - 12. \tag{4.1}$$

SENT protocol allows several formats. Figure 4.4 shows that iBooster's pedal sensor sends a 12-bit interpretation of the position. Then comes into play the following means of error detection:

- 8-bit counter
- Inverted value of the most significant nibble
- CRC-4

This configuration is very reliable because there is plenty of redundant information; thereby, reconstruction in case of errors is possible. There are other variants, like substituting the counter and the inverted most significant nibble with another 12-bit value, but that is not the case.

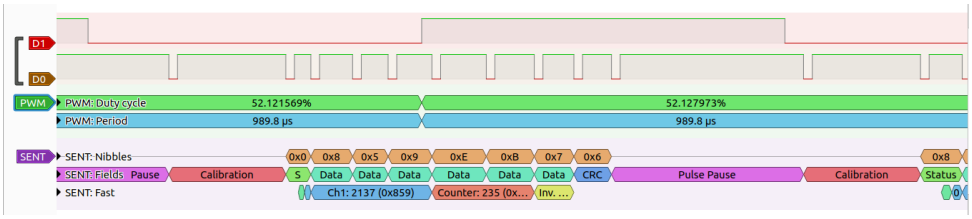

Figure 4.4: Captured communication from the pedal sensor

Moreover, the protocol improves efficiency by specializing two bits in the first status nibble. After every 16–18 transmissions on the fast channel, these two bits create a standalone slow channel message. The pedal sensor uses an enhanced message format, and table 4.2 describes the bit order and meaning.

Frame Number	Status Bit 3	Status Bit 2
1	1	CRC-6(05)
2	1	CRC-6(04)
3	1	CRC-6(03)
4	1	CRC-6(02)
5	1	CRC-6(01)
6	1	CRC-6(00)
7	0	DATA(11)
8	0	DATA(10)
9	MSG-ID(03)	DATA(09)
10	MSG-ID(02)	DATA(08)
11	MSG-ID(01)	DATA(07)
12	MSG-ID(00)	DATA(06)
13	0	DATA(05)
14	DATA(15)	DATA(04)
15	DATA(14)	DATA(03)
16	DATA(13)	DATA(02)
17	DATA(12)	DATA(01)
18	0	DATA(00)

Table 4.2: Slow channel message format used in iBooster. For details see [21]

The problem with the SENT bus was the lack of support for decoding in software for logic analyzers. There are only a few pull requests on *GitHub* that implement this bus's decoder into the *PulseView*. In the end, I used a testing version of the decoder (see [22]). Unfortunately, the ability to decode slow channel messages has not provided satisfying results in terms of the reliability for the extraction of messages efficiently. Henceforth, I walked through several hundreds of the fast messages (for detail, see appendix E) and discovered a pattern in the slow channel shown in the table 4.3.

0-0x1000	0-0x6004	0-0x1000	0-0x5006	0-0x1000
0-0x3050	0-0x1000	0-0x7000	0-0x1000	0-0x8000
0-0x1000	0-0x9000	0-0x1000	0-0xA000	0-0x1000
2-0x332B	0-0x1000	2-0x9F22	0-0x1000	2-0xAB13
0-0x1000	2-0xB874	0-0x1000	2-0xCA12	**8-0x01A3**

Table 4.3: Messages transmitted periodically on the slow channel (Notation: ID-Hex_Data)

The bold values in the table 4.3 behaved dynamically. Using this slow channel for parameters that do not change frequently, like temperature, is common practice. Also, there may be a serial or vendor identification number among the constant values.

Hence, these changes seemed minor; I replicated the sensor's output with a microcontroller, changing the 12-bit value in the fast channel and repeating the table 4.3 for the whole experiment. The PWM signal's duty was slightly more than 50 % to mimic the pedal press. The booster jerked and sometimes started moving the rod like a driver would have pressed it. This movement was unreliable, and the response time was slow. Another problem with this approach was that it required a system restart before every attempt. For all of these reasons, without the knowledge of all values and their meaning, this solution is a dead end.

Controlling the iBooster without proprietary control unit

As providing artificial data was ineffective, I dismantled the iBooster's control unit. This step allowed me to connect wires directly to the PMSM and fully control the actuator's movement. The solution's benefit lies in avoiding unpredictable scenarios in the control unit's software which could cause the failure of the method described before. Figure 4.5 illustrates the drafted scheme of the proposed control system.

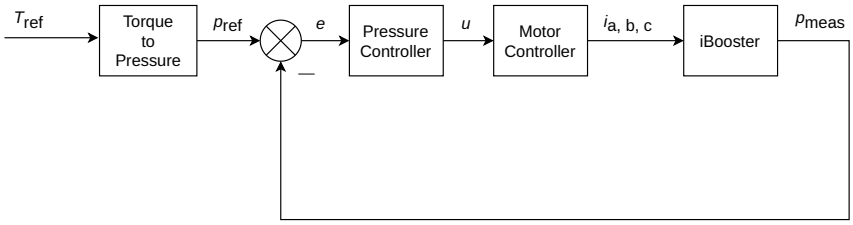

Figure 4.5: Intended software implementation of the low-level control loop

The direct connection to the motor needs a proper motor controller. Ideally, the most suitable one should guarantee an industrial-level case for protection and withstand about five amperes[1]. The controller has to support sensorless mode for PMSM because either hall sensors or an encoder are absent on

[1]Previous calculations have recommended the hydraulic pressure of 50 bars [15]. That is about five amperes, according to [17]

the iBooster. By that time, plenty of solutions by various companies on the market did not fulfill these requirements. Last but not least, the supply shortage also hit this market, including dev-kits. In the end, we dropped the condition of the durable casing and went for the SOLO UNO V2 motor controller (see [23]), depicted in the following figure 4.6.

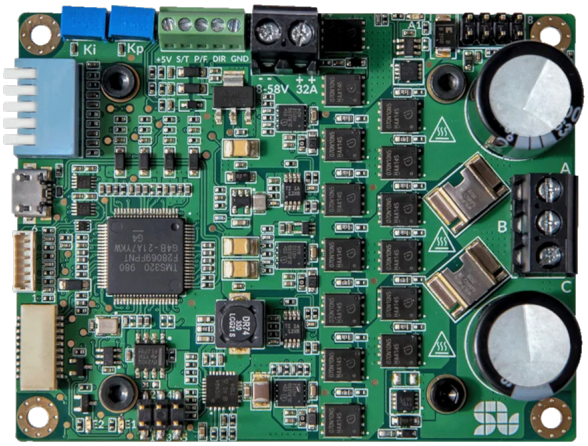

Figure 4.6: SOLO UNO V2 by SOLO Motor Controllers. Adopted from [23]

The selected motor controller meets everything we need with the maximal continuous current of 32 A. In addition to operating in both open and closed-loop modes, it supports Field Oriented Control algorithm extended for sensorless applications. It is worth noting that the controller works with other electric motors like DC or BLDC ones, making the SOLO UNO a universal solution.

Initially, I wanted to benefit from the current (torque), and speed closed loops for accurate and smooth control. The experiments with the motor controller and iBooster have shown that the sensorless mode is in the early stage and cannot reach an operating point for switching on the observer of the Field Oriented Control because of the wrong automatic identification. Thereby, I have to use the motor controller in open-loop mode to activate iBooster. That has been an involuntary decision in the design.

The simplest form of setting the desired speed and power is through the inputs on the board. The motor controller accepts analog signals in the range of 0–5 V or PWM signals with a frequency above 5 kHz. The PWM method is chosen because the microcontroller, introduced in the upcoming section 4.3.1, requires a 3.3V supply voltage. The tables 4.4 and 4.5 presents the rest of the necessary configuration settings.

Pin	Position
1	DOWN
2	UP
3	UP
4	DOWN
5	UP

Table 4.4: Piano Switch Settings

Parameter	Value
PWM Frequency	8 kHz
Motor type	BLDC
Current Limit	5 A
Number of Poles	12

Table 4.5: SOLO UNO Firmware Settings (determined empirically)

4.2 Mechanical Design

The final solution of this project should be designed with the requirement of fitting into an actual car in mind. The available vehicle is the first generation of Škoda Fabia. The main advantage is the wide availability of spare parts and the simple construction of the car. The most variable space for a custom system is the trunk. After removing the back seats, I got about 950x810 mm of area for construction.

Figure 4.7: The available space in Škoda Fabia

4.2.1 Mounting iBoosters

I mounted iBooster on its front side threads, which also hold the device in ordinary vehicles. The construction's durability is secured by opting for aluminum profiles and supporting bars. Figure 4.8 depicts the sketch of the holder, and the photo in figure 4.9 illustrates the real-world assembly.

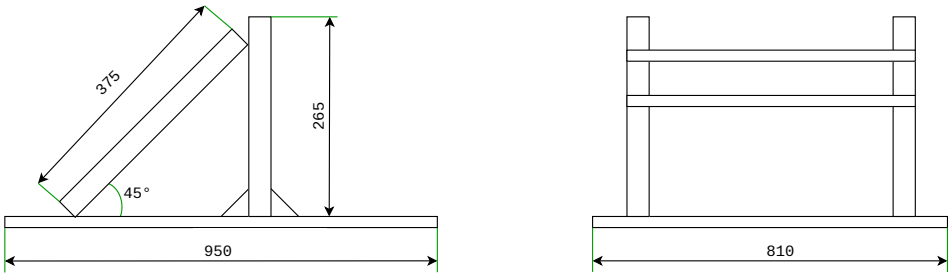

Figure 4.8: The sketch of the holder

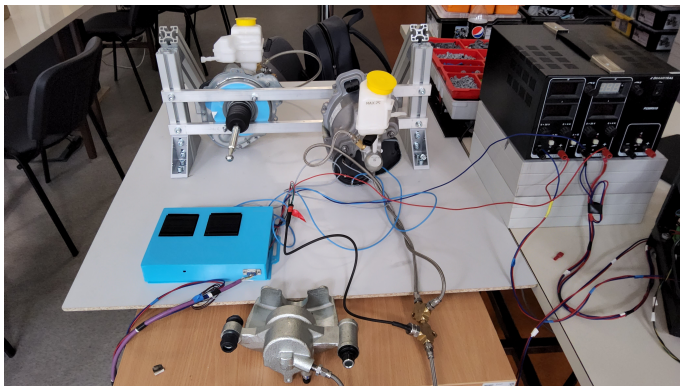

Figure 4.9: The real-world assembly

4.2.2 Hydraulic System

After mounting the iBooster, it was possible to connect the hydraulic line. The primary target is to brake with only one actuator per wheel, which requires only one brake line and can be represented by a single output of the TMC. There are two options for how to deal with the excessive output. The first is to let the brake fluid flow back to the reservoir. The latter idea considers the redundant output as the second piston for a greater force that generates brake torque. Naturally, efficiency belongs among the critical parameters in every technical solution, and thus the outputs of the tandem master cylinder are connected via a T-connector, as figure 4.10 shows. The scheme also includes a second T-connector that opens a port for a pressure sensor.

The TMC on iBooster has M12x1 threads. Because of overall compatibility with Škoda Fabia, the M10x1 threads are harmonized in the whole custom hydraulic system. Hence, TMC has a reduction from M12x1(M) to M10x1(F) added on each brake line.

Brake lines consist of two parts in vehicles. Brake pipes are made of copper or stainless steel, whose advantages are durability and lower price, and thus pipes are used to distribute brake fluid in static parts of cars. However, in my case, delivering the hydraulic pressure directly to the wheels is necessary, for which brake hoses suit better. The key factor is their flexibility in comparison to pipes. This practice can also be seen in ordinary vehicles because it is the best way to deal with moving axles and wheels.

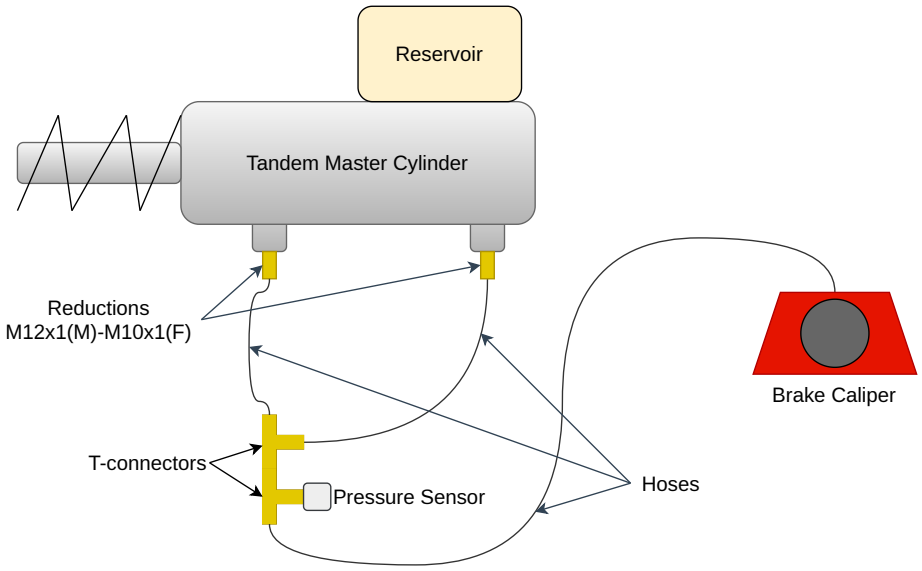

Figure 4.10: The schematics of hydraulic system

A good reason to choose hoses over pipes is the ease of assembly. Brake pipes must be bent and require special pipe flaring equipment, which I would have needed to learn from scratch. Also, once created, brake pipe redesigning brings plenty of difficulties and may even be impossible, which would limit all future placement changes. In contrast, brake hoses need only fittings whose assembly is straightforward and demand only elementary tools. That is why all hydraulic lines on the project use standard AN3 (D-03) stainless braided teflon brake hose.

4.2.3 3D-Printed Components

Everything should have its place and not be swinging around. Moreover, used electronic components do not meet any kind of protection, although these components are brittle and sensitive to unprofessional manipulation. As a solution, I modeled custom parts for a 3D printer.

The box in figure 4.11 secures the essential protection of electronics, albeit water and dust could get inside and potentially harm components inside in natural conditions; covering such a scenario is not crucial for the project's current phase, as mentioned previously. The attentive reader notices that I modeled the box upside down. This intentional decision enabled simplifying the 3D printing of holes for coolers and fixing all boards on one part for quicker wiring up. Since one of the boards has components close to its mounting holes, the box includes columns to constrain the board's position instead of screws.

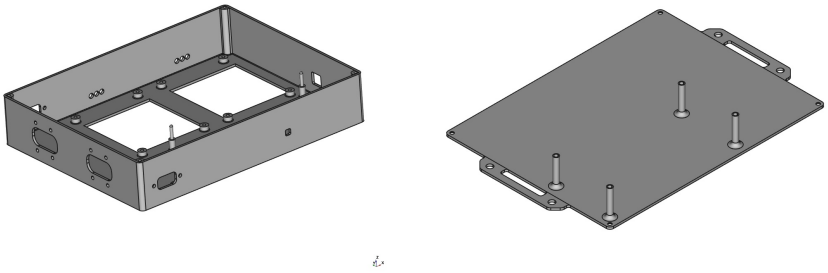

(a) : Upper part **(b) :** Lower part

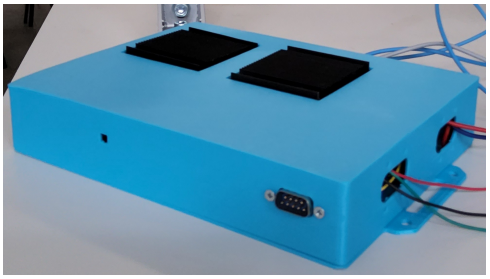

(c) : Assembled 3D-printed box for electronics

Figure 4.11: The box for circuit boards

Afterward, the T-connectors require a stand, shown in figure 4.12. I intend to use this stand only for prototyping. The real-world application demands a unique stand for every pair of T-connectors because of the nuances in thread manufacturing. As a result, the fittings align differently for every two pieces when tightened firmly. However, the stand was still able to satisfy the application's needs.

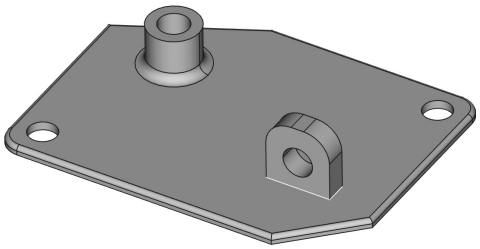

Figure 4.12: The stand for T-connectors

4.3 Electronics

Besides the motor controller, the project requires a control unit and reading from several sensors like a pressure sensor, wheel speed sensor, or a pedal unit adopted from [15]. The simplified final wiring diagram is in figure 4.13. The rest of the section offers insight into yet unmentioned blocks. Furthermore, the photo in figure 4.14 depicts the final wiring in the 3D-printed box.

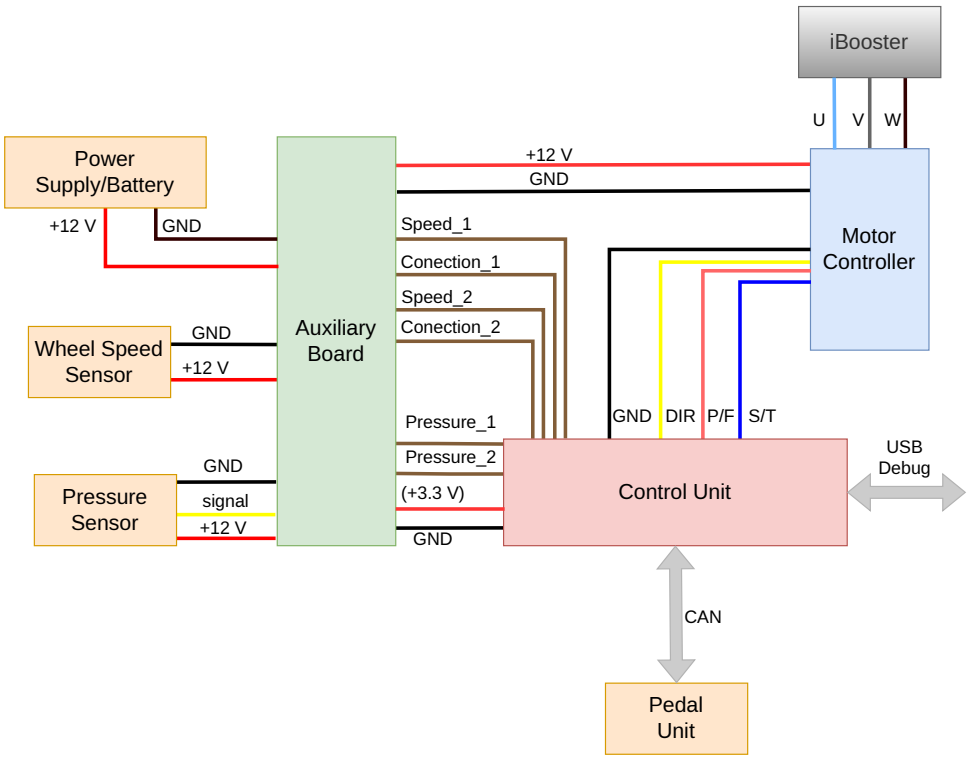

Figure 4.13: Generalized schematics of the whole electronic system

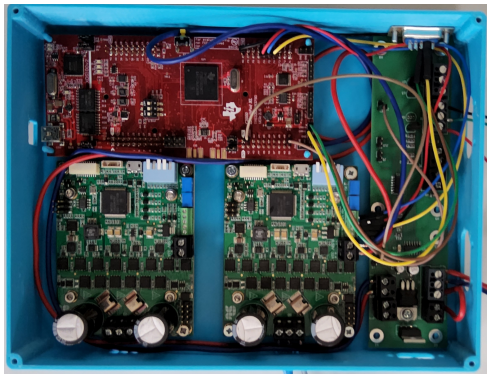

Figure 4.14: Photo of the final wiring inside of the 3D-printed box

4.3.1 Control Unit

Control algorithms may demand vast computational power and memory. Several other requirements on the control unit must be met, like the support of CAN bus, ease of data acquisition, and simple usage. As a result, the development kit LaunchPad LAUNCHXL-F28379D by Texas Instruments is used.

The LaunchPad belongs to the C2000 family of real-time microcontrollers, which offers mentioned performance and peripherals. To name a few parameters, the F28379D operates at the clock speed of 200 MHz with two C28x cores; flash memory can store up to 1 MB, and the board is able to communicate via CAN. Last but not least, the board's peripherals include 12-bit analog-to-digital converters and timers for PWM signal generation and input capture capability, which are utilized for processing outputs of sensors.

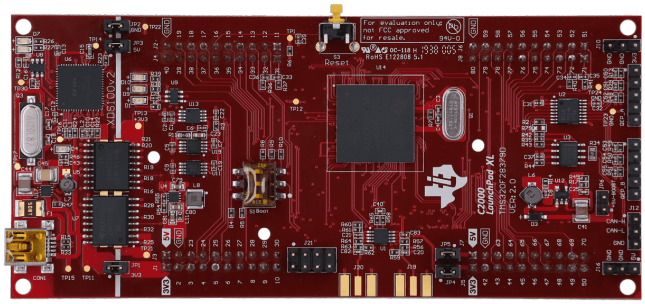

Figure 4.15: Illustrative picture of the development board. Adopted from [24]

Programming options are classic C/C++ and relatively straightforward graphical programming in MATLAB Simulink. I chose the second alternative because Simulink is software for modeling control systems. This combination is suitable for rapid prototyping and incorporates a model-based design approach, which has gained widespread recognition in the automotive industry.

Pin (Hardware)	Usage
74 (GPIO14)	I/O - DIR for SOLO
75 (GPIO11)	PWM - Speed reference for SOLO
76 (GPIO10)	PWM - Maximal power reference for SOLO
70 (ADCINA1)	Pressure

Table 4.6: Connected pins on the LaunchPad

4.3.2 Auxiliary Board

The printed circuit board serves as the space for terminal blocks to connect and redistribute data signals and power supplies between individual components. Furthermore, the board contains operational amplifiers and comparators for preprocessing signals from sensors. Additionally, there is a linear regulator from 12 to 3.3 V just in case the project would be deployed in a standalone application without debugging and power supply from the USB connection. For complete schematics and layers of the printed circuit board, see the appendix B.

4.3.3 Pressure Sensor

Hydraulic pressure in the brake line is critical information for many reasons. Above all, chapter 2 demonstrates pressure's crucial role in calculating the frictional brakes' brake torque, and both quantities are necessary for feedback control. Secondly, it would be possible to detect a malfunction in a brake line and report it to the vehicle control unit. Therefore it is necessary to add a physical sensor.

Figure 4.16: Illustrative picture of the pressure sensor. Adopted from [25]

Figure 4.16 shows the chosen sensor of hydraulic pressure. It suits the application well because it was explicitly created for brake line measurement. The sensor offers an analog output of 0.5–4.5 V. The 0.5 V offset is standard practice in the automotive industry as it facilitates electronic error detection. However, the output voltage exceeds the capabilities of the ADC. Although I do not expect a pressure of approximately 60 bar, corresponding to the 3 V, I cannot predict the behavior and performance of the iBooster. Thus I rather rescaled the voltage to 3.3 V with the circuit in figure 4.17.

Rescaling changes the relationship between the measured hydraulic pressure and the output voltage. The sensor's characteristic is linear. Consequently, the rescaling does only minor changes, as shown in figure 4.18. The equation (4.3)

Figure 4.17: The circuit designed for pressure sensors signal preprocessing

shows how to calculate pressure from a 12-bit value from ADC. For even better measurement results, readings from the sensor are filtered by Simulink's median filter with the default sliding window.

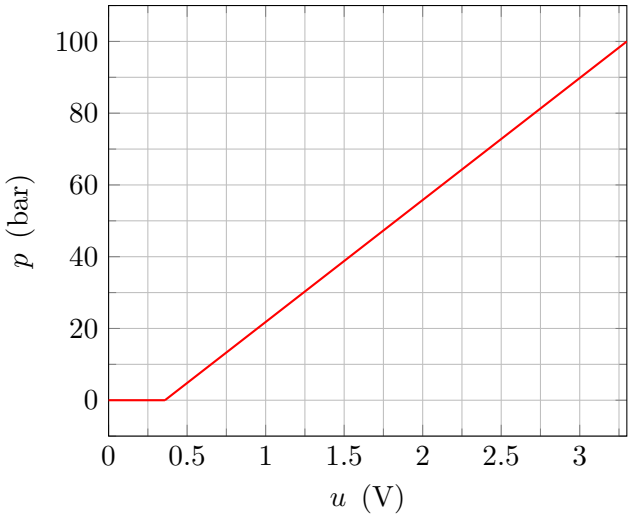

Figure 4.18: Voltage-Pressure characteristics

$$p = 34u - 12.2, \tag{4.2}$$

$$p = \frac{34 \cdot 3.3}{2^{12}} n - 12.2, \tag{4.3}$$

where p is the hydraulic pressure, u symbolizes the voltage and n is the output of the ADC.

4.3.4 Wheel Speed Sensor

In the meantime, before the iBooster units were delivered, I had spent time preparing for future implementation in the actual car. According to legislation, every modern vehicle must implement ABS. Therefore it is essential to know how to process the output of a WSS.

There are two types of WSSs on the market. The passive ones generate sine waves, and the latter, active ones, provide square wave signals thanks to the Hall effect sensor. Both solutions utilize the same principle of frequency measurement. However, the square wave signal has the advantage of easy processing with the microcontroller's input capture unit. The sensors for Škoda Fabia, which look like the one in figure 4.20, are already based on active principle.

Figure 4.19: Illustrative picture of the WSS

Similarly, the WSS output has offset like the previously introduced pressure sensor. On the other hand, the information of the WSS sensor is binary, and the sensor has current output. Due to that, the signal is connected to the 220 Ω resistor (as shown in figure 4.19), which works here as a current-to-voltage converter. The standalone resistor is less ideal than a convertor with an operational amplifier or other active components, but voltage followers compensate for this disadvantage.

The following method demonstrates how the resistance of 220 Ω is determined. I measured the current in both low I_{low} and high I_{high} states and then, according to Ohm's law:

$$I_{\text{low}} = 7.43 \text{ mA}, \tag{4.4}$$

$$I_{\text{high}} = 14.30 \text{ mA}, \tag{4.5}$$

$$R = \frac{U_{\text{cc}}}{I_{\text{high}}} = \frac{3.3}{14.30 \cdot 10^{-3}} = 231 \ \Omega. \tag{4.6}$$

After aligning with available resistors, the 220 Ω is the closest value, and the voltage levels are

$$U_{\text{low}} = 1.63 \text{ V}, \tag{4.7}$$

$$U_{\text{high}} = 3.15 \text{ V}. \tag{4.8}$$

The circuit in figure 4.20 has two parts. The upper part contains a comparator that compares sensor output with a reference voltage of 2.495 V. This voltage lies almost in the middle of values presented in eq. (4.7) and (4.8). The used comparator has an open collector output that spares a transistor. Adjusting the signal is demanded by the microcontroller's input capture peripheral (also called eCAP in the documentation and Simulink) because it can detect falling/rising edges only on conventional logic levels.

The lower part includes an operational amplifier as a voltage follower, additionally to the comparator. The decision is backed by an idea that, traditionally, non-inverting input is considered to have better (higher) input impedance. Also, it is one way to neglect the danger of input offset voltage. If we had an operational amplifier and comparator with the same offset voltage, the effect constant would appear on both sides of the comparator's inequality. The offset is not exact in this case, but they are close enough.

Moreover, the protection against offset is also secured by the 1.2 V reference voltage. This value was chosen because it satisfies the criterion that the reference voltage must be lower than 1.6 V for reliable broken wire detection with noise and voltage offsets in mind.

The wheel's angular speed can be calculated as

$$\omega = \frac{2\pi \cdot i}{N \cdot t}, \tag{4.9}$$

where N is the number of ABS teeth, and i is the number of ticks and t is a constant time window for the measurement.

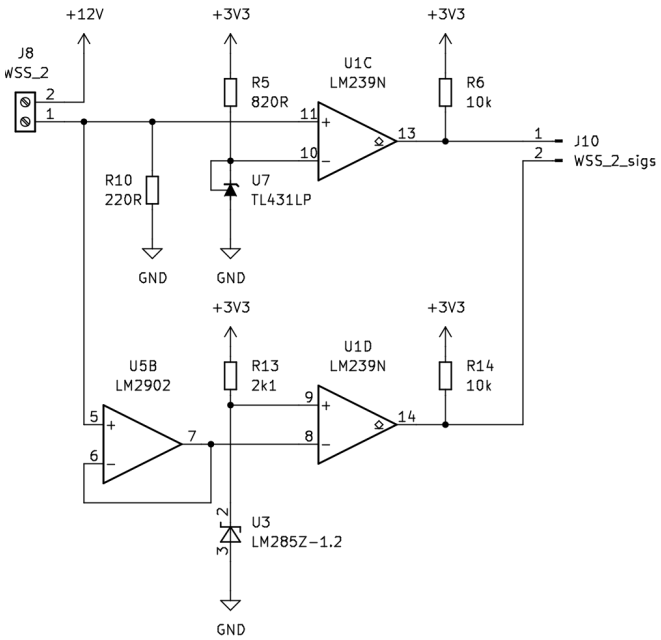

Figure 4.20: The circuit designed for WSSs signal preprocessing

Chapter 5

Control System Design

The creation of the system's model is a necessary procedure for the development of a control system. A proper and accurate model would have allowed us to use modern control design techniques and provided greater insight. Nevertheless, we did not receive any technical specifications for the iBooster; hence, it is not probable that the modern approach could deliver good results. Unknown systems like this are called black-box.

5.1 System Identification

The input into the system is the angular speed of the PMSM, and the output is the hydraulic pressure. As the position of the TMC and hydraulic pressure are closely related, I assume the system is astatic for this type of input. Astatic, also called type 1, systems identification is based on the rate of their rise over time which leads to examining an asymptotic line with the system's response.

However, even after several attempts at brake line bleeding, I could not get rid of the air in the hoses. I also witnessed minor leaks around the reductions and T-connectors. According to figures 5.1a and 5.1b, I attempted to simulate the variation of time delay and saturation.

Even more counterintuitive is that with more significant input, the system reacts with lower saturation. Also, I determined by the step responses' shapes (and then empirically tweaked) the system's gain, and based on the reaction time after the time delay, I identified the transfer function

$$G(s) = \frac{76.726}{s(s + 2.5578)} \cdot e^{-sT_\mathrm{d}}. \tag{5.1}$$

The whole system's Simulink model is depicted in figure 5.2.

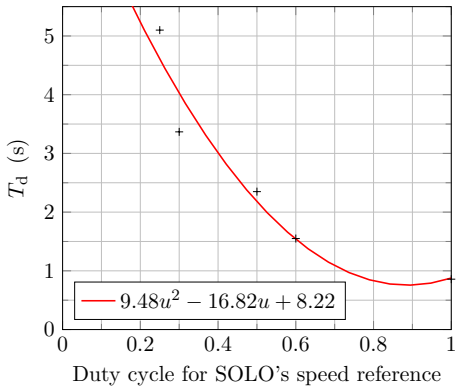

(a) : Approximation of the transport delay

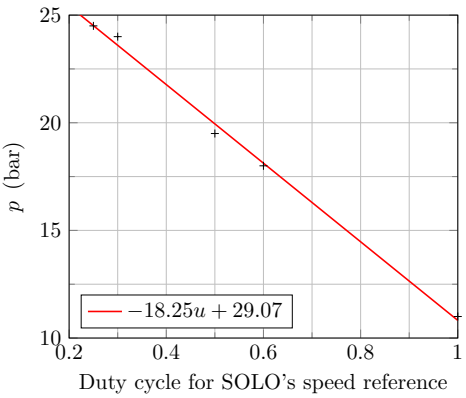

(b) : Approximation of the saturation

Figure 5.1: The Least Squares Approximations of non-linearities of the system

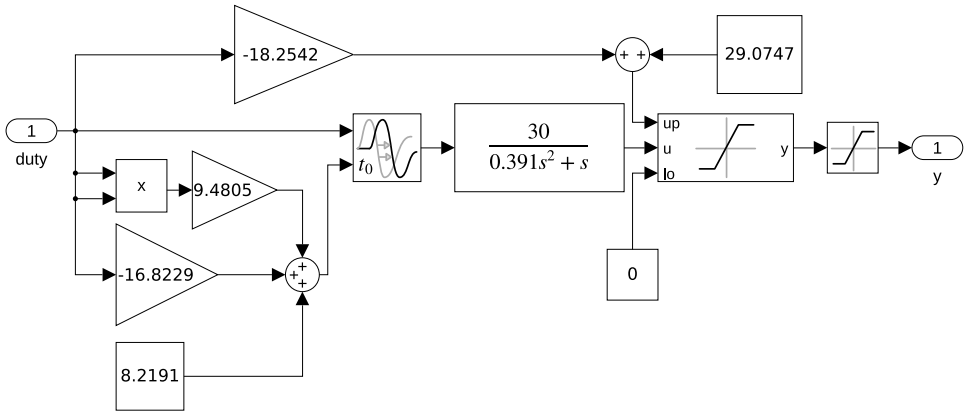

Figure 5.2: Model of the system in Simulink

Under undesirable circumstances of nonlinearities of the system probably caused by the air, the model gives promising results as presented in figures 5.3. Although the gain of the real system varies with different inputs, the error is within only half of a second. This error is tolerable because the system is slow, as the pole in eq. (5.1) indicates. The time delay lasts between a second and exceeds five seconds for low inputs, which is not ideal behavior. For the most part, the model gives a solid understanding of the real-world system and enables utilizing this insight for control algorithm design.

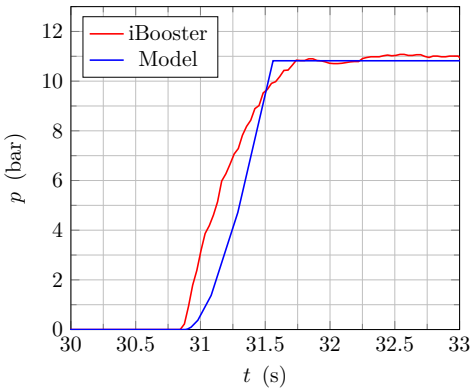

(a) : Response for $\mathbf{1}\,(t = 30)$

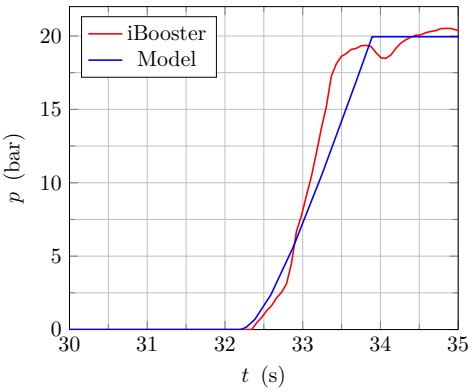

(b) : Response for $0.5 \cdot \mathbf{1}\,(t = 30)$

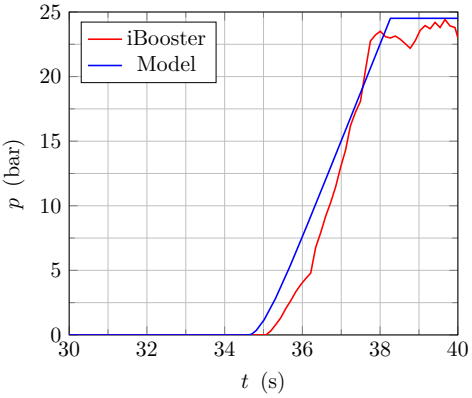

(c) : Response for $0.25 \cdot \mathbf{1}\,(t = 30)$

Figure 5.3: Open-loop step response comparison under different inputs

5.2 Software Implementation

The Simulink scheme in figure 5.4 shows the central part of the program. Because of all delays, the final hardware is not integrated into a higher-level system, and thus it lacks reporting about its state on CAN bus. This ability was present during the development phase as the MATLAB Toolbox supports debugging the code and data logging through the USB connection.

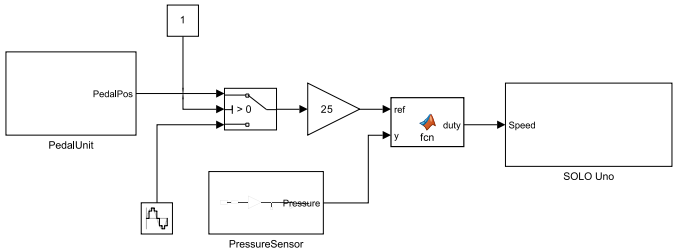

Figure 5.4: Sofware implementation in Simulink – Main body

There are several subsystems in the scheme. The first, *PedalUnit*, is adopted from [15]. The block maintains a CAN connection with the pedal unit and extracts data about the brake pedal position. Information like the throttle pedal position or brake status is discarded as it is not a matter of concern for the current project's phase. The reliably reachable pressure is approximately 25 bar; hence the 0–1 output in the message described in table 5.1 must be scaled by 25.

Sender	Message	Receiver	ID	Content
Pedal Unit	PedalUnit	Control Unit	256	Brake Position Throttle Position (Not Used) Brake Status (Not Used) Throttle Status (Not Used) Both Pedals Pressed (Not Used)

Table 5.1: Received CAN message from the Pedal Unit [15]

Then we can notice the switching between the reference from the pedal and a sine wave shown in figure 5.5. The sine wave's purpose is to replace another person's necessity during the bleeding brake lines. Whereas currently, the command during debugging activates the process, it will be replaced by a command from the vehicle control unit in the future.

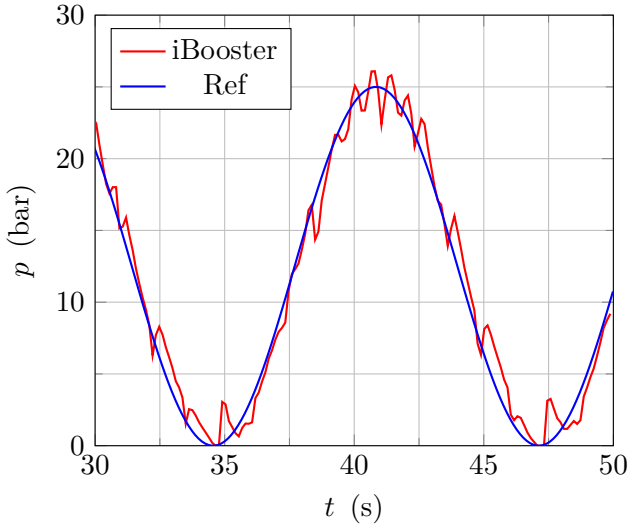

Figure 5.5: Sine wave for brake line bleeding procedure

As the name suggests, the *PressureSensor* block provides the hydraulic pressure value. Internal realization of this block does not require deeper investigation because there is just the median filter and conversion of ADC's value to pressure accordingly to the section 4.3.3.

Thence demanded and measured values are connected to the controller, implemented as a MATLAB function, which simplifies the scheme and lowers the chances of overheads with algebraic loops. For better clarity, the short

MATLAB code is provided in appendix C.

The last block, named *SOLO UNO*, is shown in figure 5.6. The ePWM block of the toolbox for the C2000 microcontroller demands a duty cycle in percentage; hence the initial step is to multiply the controller's value by 100. The requested duty cycle may be negative; thus, the absolute value block is present. The switch in the lower part works as a sign detector and determines whether the motor shall revolute clockwise or counter-clockwise. The constant PWM signal on top of the block is required by the motor controller as the maximum power protection. This duty cycle was set to allow the motor controller to draw the maximal current from the power supply and hold the motor's position.

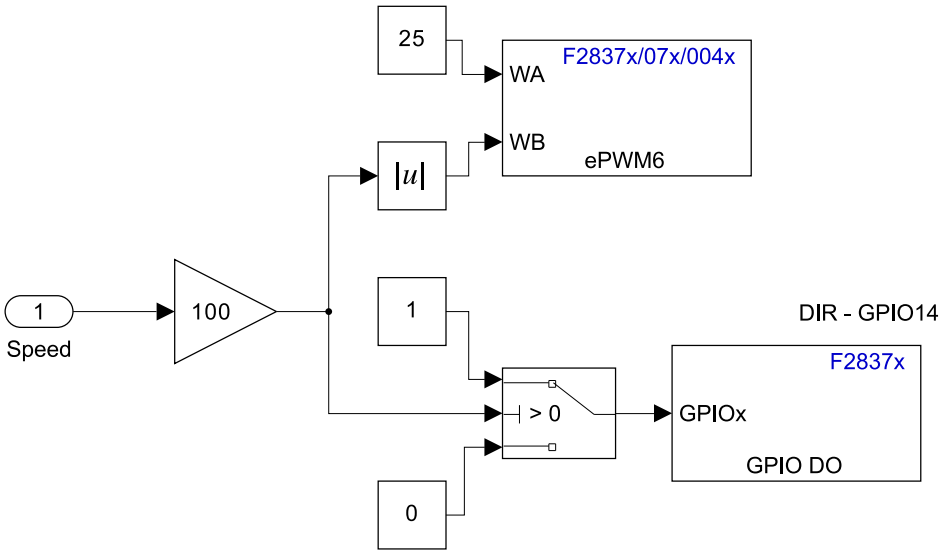

Figure 5.6: Outputs for the motor controller

5.3 Low-level Controller Design

At first, the varying saturation and time delay complicates the majority of strategies for control. The model lacks descriptivity for state-feedback control. None of the ordinary frequency domain methods, e.g., PID controller and lead-lag compensators, are suitable, as they could actuate too little or too much, lose reference tracking, and bring the whole system into undemanded oscillations. It is important to mention that the controller must consider time delay. Ordinarily, Padé's approximations or Smith's predictor mitigates constant delay in response [26], but none of these approaches suit this situation because the situation requires overcoming variable delay.

Adaptive control might solve all these struggles, but the system's diverse responses would have required a controller with plenty of operational modes. The idea of switching between regimes seems viable, and thus, I decided to implement the feedback controller with hysteresis captured in figure 5.7.

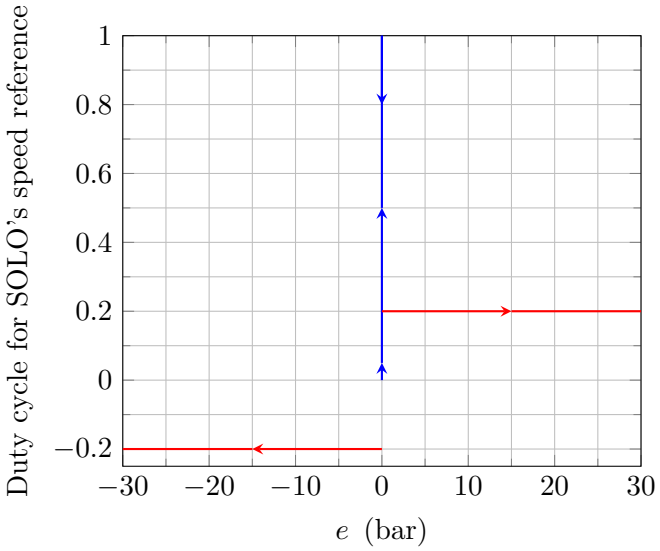

Figure 5.7: The discontinuous control signal

The controller takes advantage of the slow dynamics of the system and thus does not need a hysteresis gap because the delayed reaction replaces it. The algorithm combines two signal levels for pressing direction. If the pressure equals zero, the motor is set to maximal speed. This first step secures a quick response. When the sensor measures the first hydraulic pressure, the controller sets the duty cycle to 20 %. The lower actuation variable generates higher hydraulic pressure in the brake line before the saturation is reached. The performance of the controller is shown in section 5.4. From principle, the controller cannot track reference smoothly and will continuously oscillate around the desired value closely.

5.4 Evalutation of the Proposed Controller

The controller tracks even more complex signals like the sine wave during the brake bleeding (see 5.5) or variable step size as in figure 5.8a. Then, I tested the controller with the pedal unit to demonstrate the low-level system properties captured in figure 5.8b. Albeit all responses seem to copy well the shape of the referential signal, a closer look reveals problems with the delayed reaction. The hydraulic pressure often does not reach the demanded value before a new situation on the brake pedal arises.

The last thing to analyze is the controller's previously designed hysteresis. I claimed in the previous section that the gap in hysteresis can be neglected. The supporting argument was that this gap would allow the system's integrator to largely overshoot the requested hydraulic pressure. Even so, there are oscillations around the setpoint. Whereas I expected this behavior, I could not estimate the impacts on deceleration. For this reason, I adopted the parameters in the table 5.2 of a wheel and brake system proposed in [15].

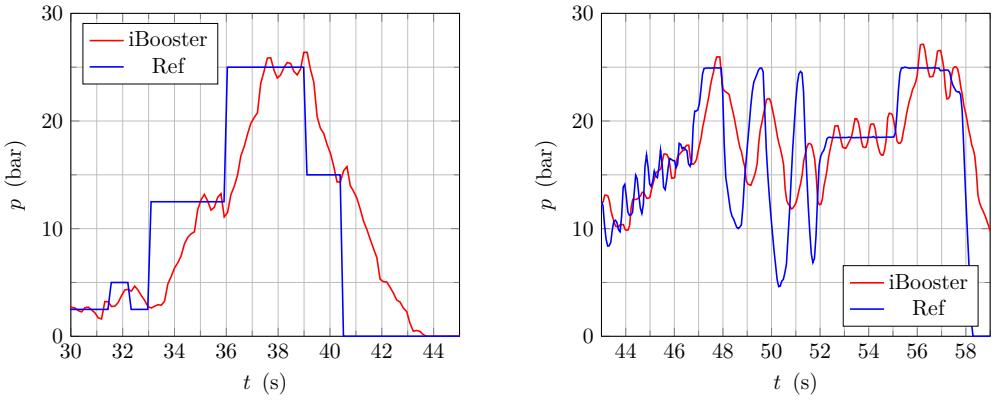

(a) : Variable unit steps

(b) : Reference from the pedal unit

Figure 5.8: Response of the closed-loop system

Parameter	Value	Description
m	1500 kg	Total mass of the vehicle
$a_{\max}$	10 ms^{-2}	Maximal deceleration
$dist$	0.65	Brake force distribution; front brakes
r_{wh}	0.321 m	Wheel radius
r_{disc}	0.17 m	Brake disc radius
h_{pad}	0.0646 m	Height of the brake pads
μ_{pad}	0.4	Brake disc-pad friction coefficient
d_{cp}	0.06 m	Caliper's piston diameter

Table 5.2: Vehicle's parameters used in the example. Adopted from [15]

From the example (3.14) presented in the section 3.4, we can calculate the swing of acceleration around the setpoint. The average error on given measurements is about 1 bar. Because the swinging is measured from peak to peak, I put $\Delta p = 2$ bar into the following equation.

$$\Delta a = \frac{\mu_{\text{pad}} \pi d_{\text{cp}}^2 \left(r_{\text{disc}} - \frac{h_{\text{pad}}}{2} \right)}{m r_{\text{wh}} dist} \cdot \Delta p = 0.398 \text{ ms}^{-2}. \tag{5.2}$$

The equation (5.2) considers the effect on the front axle. In the case of the rear axle, the swing in deceleration can be almost twice as significant because of the brake force distribution. Otherwise, an advanced high-level controller could mitigate this feature.

For the final evaluation test on a twin-track model (adopted from [12]), I decided to simplify the properties of the proposed low-level closed-loop controller. I consider the saturation to be 25 bar, constant time delay of 0.8 s, and the transfer function is based on the iBooster's response in figure 5.9. Then, the transfer function is multiplied by a constant to convert the pressure to the torque, which equals to

$$T_{\text{wh}} = 2\mu_{\text{pad}} \frac{\pi d_{\text{cp}}^2}{4} \left(r_{\text{disc}} - \frac{h_{\text{pad}}}{2} \right) p = 29.4053p. \tag{5.3}$$

The resulting transfer function for torque is

$$G(s) = 29.4053 \cdot \frac{1}{0.9078s^2 + 1.906s + 1} \cdot e^{-0.8s}. \tag{5.4}$$

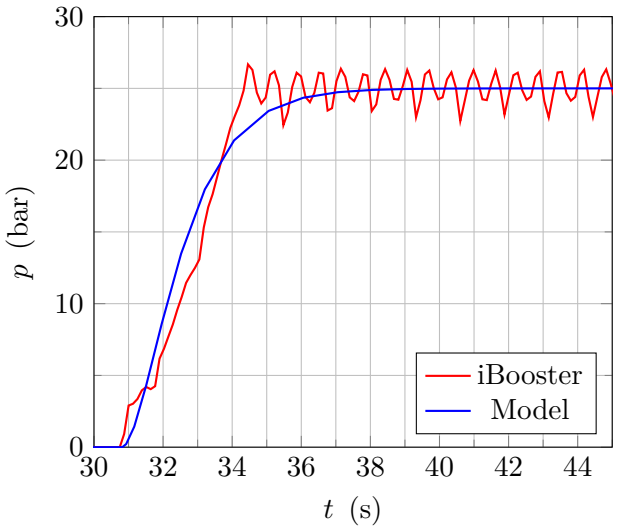

Figure 5.9: Comparison of the real and identified iBooster's response

The final test acquires data for comparison with the actuator developed in [15]. I replicated the first test - Step response, whose conditions were:

- Straightforward movement of the vehicle
- Initial speed 100 km · h^{-1}
- All wheels have the road-wheel friction coefficient set to 1
- The full deceleration (10 ms^{-2}) is applied

For the identical situation as possible, I adopted the twin-track model based on principles described in section 3 with the high-level DbW brakes control created in [12]. The parameters of the modeled vehicle are listed in appendix D.

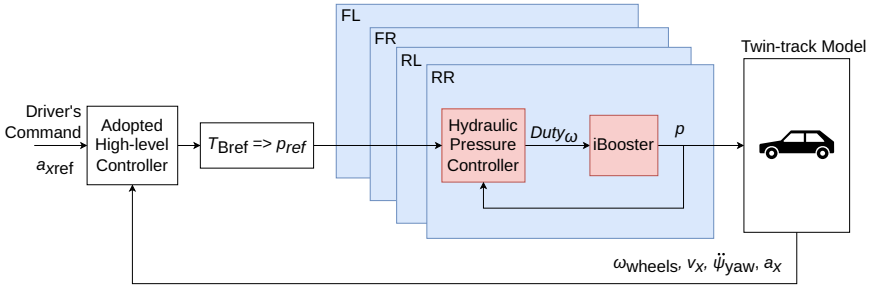

Figure 5.10: Scheme of the testing control system

The model of the modified iBooster shows promising results. The stopping distance is less than 100 m in figure 5.11b. In the high speed like 100 km · h^{-1}, it is a satisfactory result, which opens the way for considering further experiments in real-world conditions. The slips in figure 5.11d show that the car stays stable during the braking maneuver, but this happened due to ideal road conditions and limiting the movement in the straight direction.

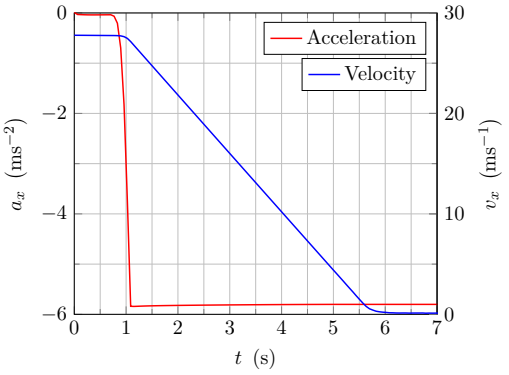

(a) : Longitudinal acceleration and velocity in time

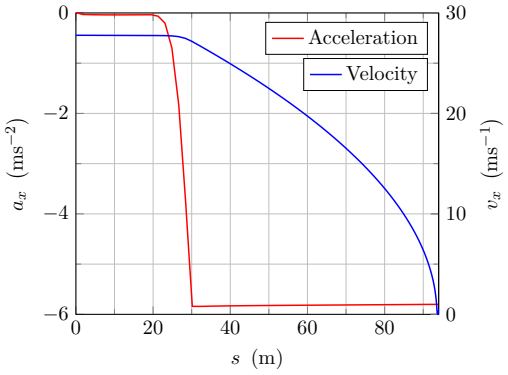

(b) : Longitudinal acceleration and velocity in distance

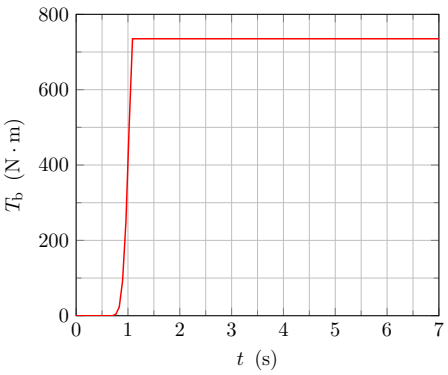

(c) : Brake torque in time domain

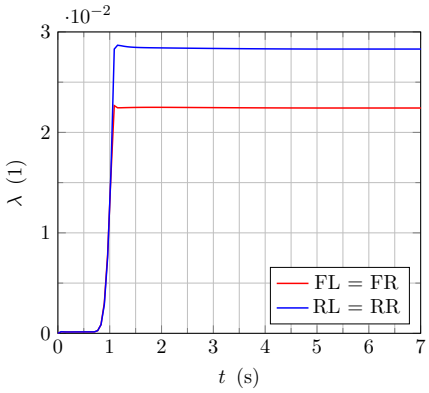

(d) : Longitudinal slips in time

Figure 5.11: Test – Step response in 100 km · h^{-1}

Chapter 6

Conclusion

6.1 Discussion of the results

The goal has been to develop and implement a modular vehicle brake system for an independent wheel. For this purpose, I examined options for controlling the acquired electric brake booster, for which I researched a solid knowledge base for future projects in Smart Driving Solutions (SDS). Although the device was received without documentation, I recognized the not that widely mentioned SENT bus and managed to decode repeating patterns in fast and slow channel messages. Despite this, I failed to analyze their entire context and figure out the state machine of the iBooster. Probably, the device cannot start without proper initialization from CAN bus. As these messages for the iBooster are available now, this theory will be investigated with the possible full communication with Bosch's proprietary control unit.

In the end, I made the electric brake booster work with the most suitable and available motor controller SOLO UNO. The final configuration struggles from the absence of cascade negative feedback in the revolution loop. Albeit the iBooster's rod moves smoothly in low load, the performance degrades in the closed hydraulic system. After considering where the original proprietary control unit acquires information about the rotor's angle for properly implemented Field Oriented Control, I concluded they likely exploit the data from position sensors and recalculate the whole internal transmission of the device.

Aside from this, I prepared utilities like circuits for sensor preprocessing, for example, WSS with the ability to detect a broken wire or sensor's power supply malfunction. Another minor subproject of this thesis is the first version of a stand for the actuators, which fits into the real vehicle's trunk and allows mounting up to two iBoosters. The construction proved to be firm and stable during all tests in the laboratory.

As section 5.4 has shown, the controller manages to stop the vehicle within the range, which is worth further experiments. The low-level hydraulic pressure control system achieved a three-second settling time for a full-scale change and about a second for minor nuances in reference. This performance is similar to the previously developed BBW unit in [15]. Yet the figure 5.11b proved that the iBooster's system's delay leads to a reaction lag, which equals about 30 m in high speed. Unfortunately, the iBooster generated only half

hydraulic pressure compared to the previous BbW unit. The high-level system managed to control the low-level model very well. Although there are still a few options for stopping the vehicle thoroughly and applying predictive control would likely make even this solution viable, the frictional brakes must be functional as a standalone braking option.

This leads to a crucial problem of the proposed solution. The hydraulics have never been bled completely. The custom-made hoses do not provide reliable sealing. It is important to mention the fittings consist of multiple parts which do not offer space for sealing rings, but there are still ways for the air left. Also, the final mounting stand for the iBooster forces the hoses to bend a lot. As a result, I suggest preferring brake pipes wherever possible in future project extensions. This statement also reflects the approach used in automotive. The brake hoses are suitable for expanding the brake line around flexible components like axles. Therefore I recommend limiting the usage of brake hoses in future development to these cases.

6.2 Future work

Because this project is a part of the larger ambition in SDS and will certainly be extended in the future, I would like to outline the following areas for improvement.

- **Hydraulic line** – I suggest replacing the brake hoses with pipes and reviewing if all connections are tightened correctly. Also, it is necessary to define the dimensions of the brake for requested brake torque to pressure conversion in the software implementation.
- **CAN Messages** – As they are available now, it is worth attempting to control the most natural way for the device. Additionally, the current custom control unit must be harmonized with the vehicle control unit for torque reference, diagnostics, and switching modes for maintenance.
- **Position sensor** – A position sensor on the booster's input rod would provide redundant information about the measured pressure.
- **ESP unit** – These lightweight actuators could be controlled via acquired CAN messages, and the saved space and weight might be worth consideration.
- **Model** – A better non-linear model of iBooster would help design an optimal controller. Although the current solution works, it would be better not to have oscillations around the reference value.
- **Consider different motor controllers** – The SOLO UNO failed to identify the PMSM by its internal algorithm appropriately. A solution with better implementation of sensorless control could improve performance and precision.

Appendix A

Bibliography

[1] M. Barrott. *Guest commentary: 2023 supply chain outlook: Buckle in for more hardships, more partnerships*. Jan. 15, 2023. URL: https://www.autonews.com/guest-commentary/supply-chain-face-more-hardships-2023 (visited on 04/09/2023).

[2] S. Korsh. *COVID-19, Supply Chain Shortages, and the Automobile Industry*. Jan. 5, 2022. URL: https://sites.lsa.umich.edu/mje/2022/01/05/covid-19-supply-chain-shortages-and-the-automobile-industry (visited on 04/09/2023).

[3] EMIS Committee meeting. *Comparative study of US and EU vehicle emissions legislation*. Institute for European Environmental Policy. Dec. 5, 2016. URL: https://www.europarl.europa.eu/cmsdata/112300/2016.12.05-Comparative%20study%20of%20US%20and%20EU%20Vehicle%20emissions%20legislation_Martin_Nesbit_IEEP.pdf (visited on 04/09/2023).

[4] The International Council on Clean Transportation. *China's stage 6 emission standard for new light-duty vehicles (final rule)*. Mar. 20, 2017. URL: https://theicct.org/sites/default/files/publications/China-LDV-Stage-6_Policy-Update_ICCT_20032017_vF_corrected.pdf (visited on 04/09/2023).

[5] The International Council on Clean Transportation. *Brazil PROCONVE L-7 and L-8 emission standards for light-duty vehicles*. Jan. 30, 2020. URL: https://theicct.org/sites/default/files/publications/Brazil_L7L8_policy_update_01302020.pdf (visited on 04/09/2023).

[6] European Commission, ed. *Regulation of the european parliament and of the council. on type-approval of motor vehicles and engines and of systems, components and separate technical units intended for such vehicles, with respect to their emissions and battery durability (Euro 7) and repealing Regulations (EC) No 715/2007 and (EC) No 595/2009*. 2022. URL: https://single-market-economy.ec.europa.eu/system/files/2022-11/COM_2022_586_1_EN_ACT_part1_v8_0.pdf (visited on 04/09/2023).

[7] B.A.P. van Duifhuizen, P.D. Hobo, H. Nijmeijer, and A. Khajepour. *Modeling, design and control of an individual wheel actuated brake system*. English. D&;C. Traineeship report. - DC 2014.052. Eindhoven University of Technology, 2014.

[8] Karl-Heinz Dietsche and Konrad Reif. *Bosch automotive handbook*. 11th. 2022. ISBN: 978-1-119-91190-6.

[9] Fred Puhn. *Brake Handbook*. HPBooks, 1985. ISBN: 0-89586-232-8.

[10] Continental. *MK C1® EVO*. URL: https://conti-engineering.com/components/mk-c1-evo/ (visited on 05/26/2023).

[11] Dieter Schramm, Manfred Hiller, and Roberto Bardini. *Vehicle Dynamics: Modeling and Simulation*. 2nd. Springer Berlin, Heidelberg, 2017. ISBN: 978-3-662-54483-9. DOI: https://doi.org/10.1007/978-3-662-54483-9.

[12] Tomáš Veselý. "ABS system modelling and control strategies development". Bachelor's. Department of Control Engineering, Czech Technical University in Prague FEE, 2020. URL: http://hdl.handle.net/10467/87766.

[13] Vít Cibulka. "MPC Based Control Algorithms for Vehicle Control". Master's. Department of Cybernetics, Czech Technical University in Prague FEE, 2019. URL: http://hdl.handle.net/10467/82396.

[14] Hans Pacejka. *Tire and Vehicle Dynamics*. 2nd. Elsevier Science & Technology, 2006. ISBN: 9780080543338.

[15] Tomáš Veselý. "Brake-by-wire system development". Master's. Department of Control Engineering, Czech Technical University in Prague FEE, 2022. URL: http://hdl.handle.net/10467/101686.

[16] *Předpis Evropské hospodářské komise Organizace spojených národů (EHK/OSN) č. 13-H – Jednotná ustanovení pro schvalování osobních automobilů z hlediska brzdění*. 2010. URL: https://esipa.cz/sbirka/sbsrv.dll/sb?DR=SB&CP=42010X0831(02) (visited on 04/29/2023).

[17] Bosch Mobility. *Technical Data - iBooster*. URL: https://www.bosch-mobility.com/media/global/products-and-services/passenger-cars-and-light-commercial-vehicles/driving-safety-systems/brake-booster/ibooster/summary-ibooster.pdf (visited on 05/01/2023).

[18] Bosch Mobility. *Operating principle of the iBooster*. URL: https://www.bosch-mobility.com/en/solutions/driving-safety/ibooster/ (visited on 05/01/2023).

[19] Armin Kunz, Michael Kunz, Herbert Vollert, and Martin Förster. "Electromechanical Brake Booster for all Drive Concepts and Automated Driving". In: *ATZ worldwide* 120.4 (2018), pp. 58–61. ISSN: 2192-9076. DOI: 10.1007/s38311-018-0009-8. URL: https://doi.org/10.1007/s38311-018-0009-8 (visited on 05/01/2023).

[20] Lars Rengersen. *Wiring the Tesla iBooster*. July 30, 2020. URL: https://www.evcreate.com/wiring-the-tesla-ibooster/ (visited on 05/01/2023).

[21] Richard Comerford. *Understanding the SENT Interface*. Sept. 11, 2014. URL: https://www.electronicproducts.com/understanding-the-sent-interface/ (visited on 05/02/2023).

[22] Jean Gressmann. *libsigrok, branch: feat_sent*. Dec. 3, 2022. URL: https://github.com/jgressmann/libsigrokdecode/tree/feat_sent/decoders/sent (visited on 05/01/2023).

[23] SOLO Motor Controllers S.R.L. *SOLO UNO_v2 User Manual - Rev. V_1.0.9*. May 2022. URL: https://www.solomotorcontrollers.com/wp-content/uploads/materials/SOLO_UNO_v2_SLU0722_5832_UserManual.pdf (visited on 05/07/2023).

[24] Texas Instruments. *LAUNCHXL-F28379D. F28379D LaunchPad™ development kit for C2000™ Delfino™ MCU*. URL: https://www.ti.com/tool/LAUNCHXL-F28379D (visited on 05/18/2023).

[25] AiM. *AiM Brake Pressure Sensor M10 0-100 Bar*. URL: https://www.aimshop.com/products/aim-brake-pressure-sensor-m10-0-100-bar (visited on 05/18/2023).

[26] Gene F. Franklin, J. D. Powell, and Abbas Emami-Naeini. *Feedback control of dynamic systems*. English. Global;Eight; New York: Pearson, 2020. ISBN: 1292274522;9781292274522;

Appendix B

Auxiliary Board

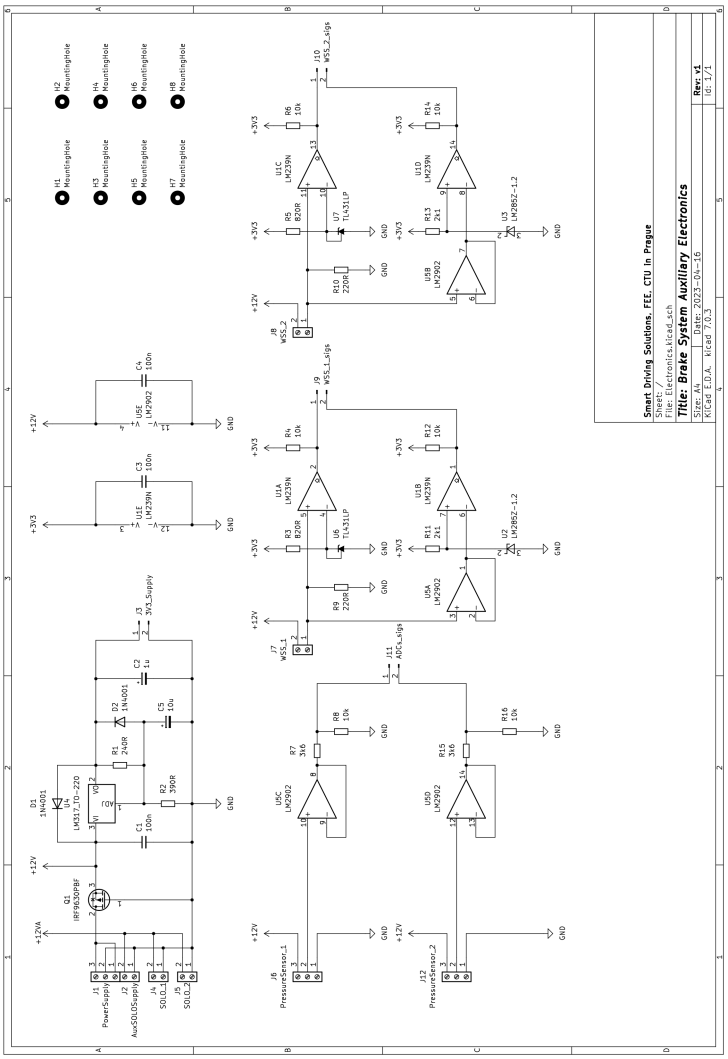

Figure B.1: Auxiliary board's full schematics

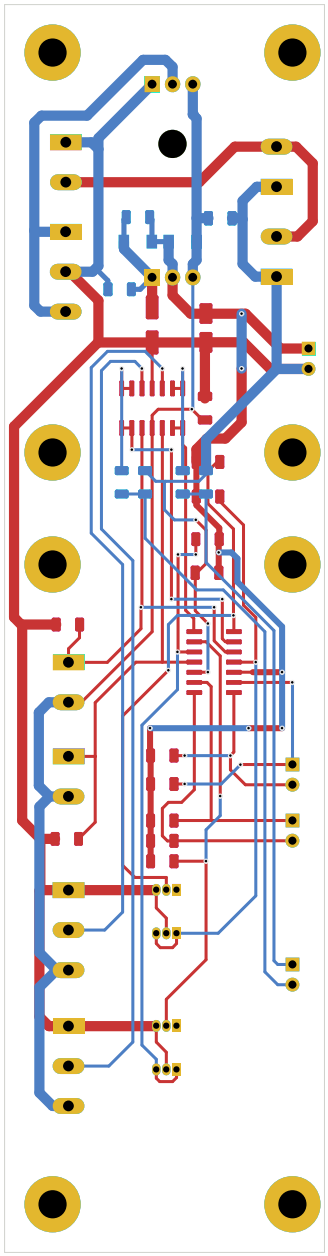

Figure B.2: Auxiliary board's PCB

Appendix C

Controller's software implementation

```
function duty = fcn(ref,y)
e = ref - y;
% No action required
if (ref == 0 && y == 0)
        duty = 0;
else
        % Slower but more precise actuation
        if e > 0
                duty = 0.2;
        elseif e < 0
                duty = -0.2;
        else
                duty = 0;
        end
        % Initial actuation for quick response
        if y == 0
                duty = 1;
        end
end
```

Appendix D

Parameters of Used Vehicle Model

Parameter	Value	Description
m	1500 kg	Mass of vehicle body
g	9.81 ms^{-2}	Gravitational constant
J_{xx}	200 $\mathrm{kg} \cdot \mathrm{m}^2$	Moment of inertia in x-axis
J_{yy}	1300 $\mathrm{kg} \cdot \mathrm{m}^2$	Moment of inertia in y-axis
J_{zz}	1400 $\mathrm{kg} \cdot \mathrm{m}^2$	Moment of inertia in z-axis
S_z	0.25 m	Vertical distance between CG and spring anchor
wheelbase	2.745 m	Wheelbase
c_w	0.18	Drag coefficient
ρ	1.22 $\mathrm{kg} \cdot \mathrm{m}^{-3}$	Air density
A	2 m^2	Area exposed to aerodynamic forces
J_ω	1 $\mathrm{kg} \cdot \mathrm{m}^2$	Wheel moment of inertia
r	0.33 m	Wheel radius
$c_{a,1,3}$	30000 $\mathrm{N} \cdot \mathrm{kg}^{-1}$	Front spring stiffness
$c_{a,2,4}$	40000 $\mathrm{N} \cdot \mathrm{kg}^{-1}$	Rear spring stiffness
$d_{a,1,3}$	8000 $\mathrm{N} \cdot \mathrm{s} \cdot \mathrm{m}^{-1}$	Front damping coefficient
$d_{a,2,4}$	8000 $\mathrm{N} \cdot \mathrm{s} \cdot \mathrm{m}^{-1}$	Rear damping coefficient

Table D.1: Vehicle body parameters. Adopted from [15]

Appendix E

List of attached files

3D_prints. . . . . . All 3D-printed models

Simulink. . . . Folder that includes software and adopted twin-track model

ibst_pedal_decoding.pdf. . The iBooster's pedal sensor decoding process